Title: Multimodal personalization of transcranial direct current stimulation for modulation of sensorimotor integration

Short title: Personalized tDCS modulates sensorimotor integration during pursuit

Radecke, Jan-Ole[a,b,*], Kühn, Alexander[a,b], Erdbrügger, Tim[c,d], Buschermöhle, Yvonne[c,e], Rashidi, Sogand[a,b], Stöckler, Hannah[a,b], Sack, Benjamin[a,b], Borgwardt, Stefan[a,b], Schneider, Till R.[f], Gross, Joachim[c,e], Wolters, Carsten H.[c,e], Sprenger, Andreas[b,g,h] & Lencer, Rebekka[a,b,e,i]

[a] Department of Psychiatry and Psychotherapy, University of Lübeck, 23562 Lübeck, Germany
[b] Center of Brain, Behavior and Metabolism (CBBM), University of Lübeck, 23562 Lübeck, Germany
[c] Institute for Biomagnetism and Biosignalanalysis, University of Münster, 48149 Münster, Germany
[d] Institute for Analysis and Numerics, University of Münster, 48149 Münster, Germany
[e] Otto Creutzfeldt Center for Cognitive and Behavioral Neuroscience, University of Münster, 48149 Münster, Germany
[f] Department of Neurophysiology and Pathophysiology, University Medical Center Hamburg-Eppendorf, 20246 Hamburg, Germany
[g] Department of Neurology, University of Lübeck, 23562 Lübeck, Germany
[h] Institute of Psychology II, University of Lübeck, 23562 Lübeck, Germany
[i] Institute for Translational Psychiatry, University of Münster, 48149 Münster, Germany

[*] Corresponding author at: Department of Psychiatry and Psychotherapy, University of Lübeck, Ratzeburger Allee 160, 23562, Germany

Declarations of interest: None.

Acknowledgements: This work was supported by the German Research Foundation (DFG; WO1425/10-1 to CHW, GR2024/8-1 to JG and LE1122/7-1 to RL) and by the Bundesministerium für Gesundheit (BMG; ZMI1-2521FSB006, under the frame of ERA PerMed as project ERAPERMED2020-227). JG was further supported by the DFG (GR2024/11-1, GR2024/12-1, TRR393). JOR was funded by the Clinician Scientist program of the Section of Medicine of the University of Lübeck. We thank Dr. Martin Göttlich and Andreas Wollbrink for technical support, Karin Wilken, Hildegard Deitermann, Ute Trompeter, Susanne Schellbach and Mandy-Josephine Reichhardt for support with the data acquisition, and Prof. Peter Trillenberg for helpful discussions.

Multimodal personalization of transcranial direct current stimulation for modulation of sensorimotor integration

Abstract

Transcranial direct current stimulation (tDCS) for the modulation of ongoing eye movements provides an ideal model for investigating sensorimotor integration. Within neural networks subserving smooth pursuit eye movements, visual motion area V5 is a core hub to integrate visual motion information with oculomotor control. Here, we applied personalized tDCS explicitly targeting individual V5 in healthy human participants using algorithmic optimization informed by functional magnetic resonance imaging and combined electro- and magnetencephalography. We hypothesized subtle modulation of sensorimotor integration during pursuit and assessed the gain by personalized tDCS targeting V5, compared to personalized tDCS targeting the frontal eye field, as well as conventional normative tDCS over V5. Indeed, pursuit initiation was specifically delayed during personalized cathodal tDCS targeting right V5 indicating the involvement of distinct functional subregions of V5 in the initial sensorimotor integration of visual motion information with pursuit eye movements, but not the maintenance of ongoing pursuit. The results were well-controlled by anodal and sham tDCS, different pursuit tasks, finite-element simulations of individual electric fields, and by two additional control experiments, one that applied personalized tDCS targeting frontal eye field and another that applied normative tDCS over V5. Importantly, in contrast to personalized tDCS targeting FEF and normative tDCS over V5, personalized tDCS targeting V5 effectively modulated pursuit by adapting electric fields to individual anatomical and functional V5 properties. Our results provide evidence for the specific involvement of area V5 in sensorimotor integration during pursuit initiation and the ability of (targeted) tDCS to specifically introduce subtle modulation of the brain network underlying smooth pursuit eye movements. Further, our results indicate the potential of personalized tDCS to alter behavior as the main aspect of interest in human neuromodulation.

Keywords: non-invasive brain stimulation (NIBS); individualized transcranial electric stimulation (tES); oculomotor; human MT+; sensorimotor transformation; targeted transcranial brain stimulation (TBS)

Abbreviations: SP: Smooth pursuit eye movements; tES: transcranial electric stimulation; tACS: transcranial alternating current stimulation; tDCS: transcranial direct current stimulation; FEM: finite element method; DWI: diffusion weighted imaging; MRI: magnetic resonance imaging; EEG: electroencephalography; MEG: magnetoencephalography; MEEG: combined EEG and MEG; FEF: frontal eye field; BOLD: blood oxygen level dependent; SMS: simultaneous multislice; TRI: continuous pursuit task; LCMV: linearly-constrained minimum variance; DCMI: distributed constrained maximum intensity; TRIBL: continuous pursuit task with blanking; SR: foveopetal step-ramp task; LMM: linear mixed model; MT: middle temporal visual area; MST: medial superior temporal area;

1. Introduction

Smooth pursuit eye movements (SP) significantly shape our daily interactions with the environment [1] and provide an ideal model for studying sensorimotor integration mechanisms [2,3]. Based on the temporal dynamics of pursuit and the involved brain regions, SP initiation is typically dissociated from sustained SP maintenance. As part of the neural network underlying eye movement control [4,5], the extrastriate visual motion area V5/MT+ [6] has been identified as a key hub for the integration of visual motion processing during both SP initiation and maintenance [2,7–12].

Animal physiology studies demonstrated that the initiation of SP is predicted by activity in the V5-equivalent area MT+ [12–15]. Furthermore, lesion studies of MT+ in macaque monkeys demonstrated impaired SP initiation and maintenance [16–19]. This evidence is complemented by microstimulation of MT+ that increased SP velocities towards the stimulated hemisphere (i.e., ipsiversive SP), and decreased contraversive eye velocities [10]. Accordingly, human lesion studies including area V5 have demonstrated both impaired SP initiation and maintenance [20–22]. In line with this, suprathreshold neuromodulation by transcranial magnetic stimulation (TMS) targeting right V5 in humans induced an overall decrease of ipsiversive (i.e., rightward) SP velocity [23]. Furthermore, functional imaging studies associated activity in the human area V5 with SP stimulus velocity on the one hand as well as the corresponding eye velocity on the other hand, with pronounced V5 activity in the right hemisphere, compared to the left hemisphere [24–26].

Subthreshold neuromodulation of V5 in the healthy brain provides an interesting model for a better understanding of the role of V5 for SP [27]. Furthermore, such techniques can be used to mimic subtle functional impairments of sensorimotor integration, observed in the elderly or clinical populations [28–34]. More specifically, subtle subthreshold

104 neuromodulation by transcranial electric stimulation (tES), including direct current (tDCS) and
105 alternating current stimulation (tACS) can induce transient online-effects and after-effects
106 that outlast the actual stimulation. Several studies induced altered visual motion processing
107 using tDCS or tACS [35–40], but the effect of tDCS on sensorimotor transformation remains
108 elusive. To our knowledge, only one recent study applied normative tDCS over V5 [27] to
109 explicitly modulate sensorimotor integration during SP but did not describe tDCS-induced
110 changes of SP performance.

111 Conventional tDCS, and tES in general, suffers from a high proportion of non-responders
112 [41–43] and overall small effect sizes in meta-analyses [44,45]. This may partly be explained
113 by the fact that conventional tDCS uses the identical normative scalp electrode montage
114 across subjects. However, based on extensive research on finite element method (FEM)
115 simulations of individual transcranial electric fields [46], it has been shown that, due to volume
116 conduction, inter-individual anatomical differences shape individual tES electric fields that
117 vary near the putative effective threshold to induce subthreshold neural modulation [46–49].
118 Importantly, neurophysiological markers of tES effects [50–52] and behavior [53–55] have
119 been related to individually simulated electric fields as the putative effector of tES. Based on
120 these challenges of normative tES, it has been suggested to use algorithmic optimization to
121 personalize tES montages, based on explicit assumptions about the individual anatomy and
122 target properties [46,56–58] to control individual transcranial electric fields [59,60]. In the
123 above-mentioned study [27], although no SP modulation by tDCS was described, FEM
124 simulations of transcranial electric fields indicated low directional intensities for the applied
125 normative montage that were significantly smaller compared to personalized electric field
126 intensities. However, actual experimental applications of personalized tES remain sparse

127 [53,61–63], probably due to the resource-intensive approach and, consequently, limited
128 examples for the actual gain of personalized compared to normative tES.

129 In the present study we applied personalized multichannel tDCS targeting V5 in the right
130 hemisphere (experiment 1) to specifically modulate V5-associated SP initiation and
131 maintenance of ipsiversive (i.e., rightward) SP (Fig. 1). We tested this hypothesis by explicit
132 definition of the individual target V5 and realistic anatomical head models (structural MRI and
133 diffusion weighted imaging, DWI) to compute personalized tDCS montages and thus
134 individually targeted and algorithmically optimized tDCS electric fields. Functional magnetic
135 resonance imaging (MRI) was employed to estimate individual V5 target location and
136 combined electro- (EEG) and magnetoencephalography (MEG; combined MEEG) to estimate
137 target orientation. We assessed the effect of personalized anodal, cathodal and sham tDCS on
138 different aspects of sensorimotor integration during SP, namely SP initiation (as assessed by
139 the step-ramp task, SR), maintenance of continuous SP (TRI task), and top-down control of SP
140 during continuous pursuit with blanking (TRIBL task; Fig. 1 and S3). We hypothesized
141 antagonistic effects of personalized cathodal versus anodal tDCS targeting V5 on ipsiversive
142 SP initiation and maintenance that builds up during tDCS (online-effects) and outlasts the
143 actual stimulation (after-effects). Furthermore, two control experiments were included to test
144 a) the spatial specificity of tDCS targeting V5 compared to personalized tDCS targeting the
145 right frontal eye field (FEF; experiment 2), b) effects of the personalization procedure per se
146 by personalized tDCS targeting remote FEF (experiment 2), and c) the gain by personalized
147 tDCS targeting V5 compared to normative tDCS over V5 (experiment 3). Finally, individual FEM
148 electric fields simulations were analyzed to substantiate experimental findings in an
149 independent analytical way.

150 We aimed to assess the effects of novel multimodally personalized tDCS targeting area
151 V5 for the subtle neuromodulation of SP behavior. Indeed, in contrast to personalized tDCS
152 targeting FEF and normative tDCS over V5, cathodal personalized tDCS targeting right V5
153 specifically modulated sensorimotor integration during SP initiation, but not SP maintenance
154 during ongoing eye movements. The multimodal personalization and analysis of tDCS electric
155 fields ensured the control of observed inter-individual anatomical and functional variability.
156 Further, results from three experiments allowed conclusions about the distinct involvement
157 of V5 in the modulation of SP initiation, specifically by personalized tDCS targeting this area.

158

159 ## 2. Results

160 ### 2.1 Personalized tDCS adapts to inter-individual target variability

161 Individual stimulation targets showed varying location and orientation (Fig. 2A-B).
162 Specific SP-related BOLD activity was observed in individually estimated V5 locations near
163 previously reported V5 coordinates (x/y/z MNI-coordinates, V5: 45/-67/2 ± 3/6/4; Tab. S1)
164 [7,64]. Individual V5 activation maxima deviated by 7 ± 3 mm to the mean location, yielding a
165 considerable inter-individual variability of tDCS target locations (Fig. 2B). Second-level analysis
166 of BOLD activity revealed a significant increase of V5 activity during continuous pursuit,
167 compared to fixation in a cluster in inferior and middle occipital, as well as middle and inferior
168 temporal cortex of the right hemisphere (cluster size k = 97, cluster p = .007, local maximum:
169 42/-73/2, t_{18} = 7.6) [65]. For illustration, individual statistical maps from the Pursuit versus
170 Fixation contrast were interpolated on the MNI brain, and FDR-corrected one-sample t-tests
171 are shown (Fig. 2A). A mask of the V5-equivalent cytoarchitectonic area hOc5 was additionally
172 applied and confirmed a significantly increased BOLD activity in V5 during SP compared to
173 fixation (t_{18} = 6.3, p < .001, center coordinates: 45/-61/2) [6]. In line with the heterogenous

174 cortical structural organization of V5, the estimated stimulation target orientations showed a
175 variety of quasi-radial, and quasi-tangential orientations across participants (Fig. 2B).
176 Personalized tDCS montages targeting individual right V5 confirmed a clear adaptation
177 to the target location and orientation, placing cathodes on the scalp roughly over the target
178 in the direction of estimated target orientation. Across subjects, exemplary for the application
179 of personalized cathodal tDCS, a cluster of anodes was observed including electrode positions
180 P6, P8, and CP6, whereas a cluster of cathodes was observed including electrode positions
181 PO8, PO10, O2, and O10. However distinct target orientations and quasi-radial target
182 orientations are reflected by varying tDCS electrode positions across the scalp (Fig. 2C) [60].
183 Overall SP performance was high in the expected range for young healthy participants (Tab.
184 2, see Supplement) [27].
185
186 **2.2 Personalized tDCS targeting V5 specifically modulates pursuit initiation**
187 Personalized tDCS was applied to modulate SP performance depending on tDCS
188 condition (sham, anodal, cathodal), timepoint (t_0, t_{TDCS_5}, t_{TDCS_10}, t_{TDCS_15}, t_{TDCS_20}, t_{15}, t_{40}) and
189 SP stimulus direction (leftward, rightward). Personalized tDCS targeting V5 specifically
190 modulated SP latencies in the SR task, as revealed by an omnibus analysis (three-way
191 interaction: p = .044; Fig. 3A-C, Tab. S2). Additional LMM analyses indicated an online effect
192 during tDCS (p = .015; Fig. 3A-C, Tab. 3), but no tDCS after-effects (p = .484; Tab. 4). Specifically
193 personalized cathodal tDCS delayed rightward SP latencies for t_{TDCS_20}, relative to t_{TDCS_5} (p
194 = .002, d_z = 0.93). A follow-up analysis confirmed that overall SP latencies across all timepoints
195 of the sham session (t_0, t_{TDCS_5} to t_{TDCS_20}, t_{15}, t_{40}) were delayed for leftwards compared to
196 rightwards SP (p = .007, d_z = 0.64; compare Fig. 3A), indicating that personalized cathodal tDCS
197 targeting the right V5 hampered latencies of rightward SP to the level of initially delayed

198 leftward SP latencies. In addition, a paradoxical effect by personalized cathodal tDCS was
199 observed during t_{TDCS_15} between leftward and rightward SP latencies (p = .002, d_z = 0.89) and
200 latencies for leftward SP during t_{TDCS_15} were significantly delayed for personalized cathodal
201 tDCS, compared to sham (p = .042, d_z = .72; Fig. 3A).

202 To follow-up tDCS online effects for rightward SP latencies (Fig. 3A), these were defined
203 both as difference between the first and last timepoint during t_{TDCS} ($t_{TDCS_20} - t_{TDCS_5}$; 18 [12,
204 29] ms, bootstrapped mean and [95%-confidence interval]; Fig. 3B), as well as the slope of a
205 linear fit across all four t_{TDCS} timepoints (t_{TDCS_5} to t_{TDCS_20}; 4.9 [2.8, 8.3] ms/5 minutes ; Fig. 3C).
206 While the difference tDCS effect can be directly related to the significant post-hoc contrasts
207 of the LMM analysis, the slope tDCS effect yields a more robust estimate considering the
208 paradoxical effect but thereby introduces potential noise from the SP latencies observed
209 during t_{TDCS_10} and t_{TDCS_15}. Therefore, we consider the difference and slope estimates of the
210 tDCS effect as complementary. Significant differences between personalized anodal and
211 cathodal tDCS for the rightward SP latencies were revealed for both difference (z = -3, p = .008,
212 d_z = 0.72) and slope estimates (z = -2.58, p = .03, d_z = 0.61) of tDCS effects. In addition,
213 difference tDCS effects differed between leftwards and rightwards SP latencies during
214 personalized cathodal tDCS (z = -2.41, p = .024, d_z = 0.59). The corresponding effect for the
215 slope estimate did not survive Bonferroni-correction (p = .11). In addition, the difference tDCS
216 effect was significantly larger for personalized cathodal tDCS targeting V5, when compared to
217 personalized tDCS targeting FEF (z = 2.08, p = .019, d_z = 0.5) while the same effect for the slope
218 estimate missed significance (p = .057).

219 During tDCS, an online effect on initial acceleration was also observed (p = .02; Tab. 3),
220 however, this effect was not indicated by the preceding omnibus analysis and post-hoc tests
221 did not survive correction for multiple comparisons.

222 Besides the modulation of SP latencies, no specific tDCS effects (i.e., tDCS condition *
223 timepoint or tDCS condition * timepoint * direction interaction effects) were observed for
224 tasks indicating sustained SP maintenance performance with continuously visible targets (TRI),
225 top-down mechanisms involved in ongoing SP with temporary target blanking (TRIBL) or
226 ongoing SP performance during the SR task following SP initiation (all $p > .523$; Tab. 3-4, Tab.
227 S2). Furthermore, neither personalized tDCS targeting the right FEF as a control region (within-
228 group, $p = .862$; Fig. 3D-F, Tab. S4), nor normative tDCS over V5 ($p = .93$; between-group,
229 matched sample of N = 19; Fig. 3G-I, Tab. S5) induced a modulation of SP latencies during tDCS
230 comparable to the observed effects for personalized tDCS targeting V5 (Fig. 3A-C). Finally, the
231 results were not compromised by individual tDCS side-effects (see Supplement).
232
233 **2.3 Personalized tDCS targeting V5 increases tDCS efficacy compared to normative tDCS over**
234 **V5**
235 To evaluate the electric field differences presumably leading to distinct tDCS effects,
236 electric field simulations were compared between the applied personalized tDCS targeting V5
237 and the normative V5 montage for the N = 19 subjects from experiment 1 (personalized V5;
238 Fig. 2C-F). Electric field simulations showed comparable target intensities ($p = .209$, normative
239 $|E|_{IT} = 0.62 \pm 0.38$ V/m, personalized $|E|_{IT} = 0.66 \pm 0.45$ V/m, M ± SD). However, normative
240 electric fields across the cortex showed significantly increased intensities in non-target dorsal
241 and medial parts of bilateral parietal cortex compared to personalized electric fields. In
242 contrast, personalized electric fields showed increased intensities in the right lateral occipital-
243 parietal-temporal cortex compared to the normative electric fields (Fig. 2F). In addition,
244 directionalities were significantly increased for personalized compared to normative electric
245 fields ($z = -4.87$, $p < .001$, $d_z = 1.11$; normative $|E|_{DIR} = 0.05 \pm 0.32$ V/m, personalized $|E|_{DIR}$ =

246 0.42 ± 0.28 V/m, M ± SD; Fig. 2F). Electric field spatial extent was significantly decreased for
247 personalized, compared to normative tDCS (z = 6.81, p < .001, d_z = 1.74 normative $|E|_{EXTENT}$ =
248 70 ± 2 mm, personalized $|E|_{EXTENT}$ = 57 ± 8 mm, M ± SD; Fig. 2F). In conclusion, personalized
249 electric field topographies were shifted towards individual tDCS targets in the right V5, thus
250 effectively considering the varying individual tDCS target locations and orientations in the right
251 V5 and reducing co-stimulation of non-target parietal cortex, compared to the normative
252 electric fields.

253 Indeed, the evaluation of tDCS effects on ipsiversive SP latencies revealed significantly
254 increased tDCS effects for personalized cathodal tDCS targeting V5 compared to normative
255 tDCS over V5 (difference tDCS effect: z = 2.1, p = .018, d_s = 0.7; slope tDCS effect: z = 1.81, p
256 = .036, d_s = 0.61).

257

258 ## 3. Discussion

259 We conducted a comprehensively controlled experiment to assess the effects of
260 personalized tDCS targeting V5 on SP initiation and maintenance as a direct behavioral read-
261 out of tDCS effects on sensorimotor integration. We found a spatially and functionally specific,
262 significant modulation of SP initiation by personalized cathodal tDCS that was absent during
263 anodal or sham tDCS. This effect was independent from possible practice effects [27] and tDCS
264 side-effects (Supplement). Furthermore, electric field simulations and a control experiment
265 applying normative tDCS over V5 signify more precise electric fields and an increased gain by
266 personalized tDCS in contrast to normative tDCS.

267

268 ### 3.1 Personalized tDCS targeting V5 specifically modulates pursuit initiation

269 To interpret our key finding of specific SP initiation modulation (i.e., SP latencies) by
270 personalized cathodal tDCS, it is important to consider the multimodal role of the human
271 visual area V5/MT+. V5 can be functionally dissociated into the middle temporal visual area
272 (MT) and the medial superior temporal area (MST) [7,9]. In the macaque monkey, it has been
273 shown that MT receives bottom-up visual information [66,67] and integrates these to signal
274 visual motion on the retina as a velocity signal during SP [11]. MST receives projections from
275 MT [67] and MST itself maintains reciprocal connections to various visual areas, as well as
276 parietal and premotor nodes of the oculomotor network [66,68] that govern top-down signals
277 during ongoing SP, e.g., predicting target motion even in the absence of a visual target [11].
278 Importantly, neural activity in MT+ is involved in SP initiation, but relies on gain control by
279 higher-order network nodes such as the FEF [12,13,15]. In line with these studies, human
280 V5/MT+, comprising putative MT and MST, has been suggested as a key hub for the
281 sensorimotor transformation during SP [7,69], thus integrating bottom-up visual motion
282 information with top-down oculomotor control during SP initiation and SP maintenance.
283 In the present study, SP initiation (SP latency in the SR task) was hampered by
284 personalized cathodal tDCS targeting V5. The observed impairment of ipsiversive, but not
285 contraversive, SP is in line with previous TMS modulation of the right V5 in humans [23].
286 Animal studies described an impairment of ipsiversive SP for foveopetal step-ramps after
287 lesions of the foveal representation of MT [17,19] anduman lesion studies including V5
288 described similar ipsiversive SP deficits [20–22]. However, the same authors also differentiate
289 contralesional SP deficits (retinotopic) from directional deficits that affect SP ipsiversive to the
290 lesion site [17,20–22]. During the step of the applied SR task, the visual target is moved 2.5 °
291 to one side, before it starts to move in the opposite direction with a constant velocity ramp.
292 This paradigm allows subjects to start pursuit without an initial saccade as soon as the visual

target crosses the point of the subject's central fixation at the start of each trial. However, this also implies that in the time between the step onset and the midline-crossing of the visual target, subjects fixate the center of the screen and thus are presented a retinotopic visual stimulus moving from the step eccentricity towards the participant's central fixation, before the visual target is then fixated during the actual pursuit. Thus, in the present experiment personalized cathodal tDCS presumably induced retinotopic deficits that affected sensorimotor transformation after the leftward target step onset moved the visual target to the hemifield contralateral to the targeted right V5, but before the onset of rightward SP. This would explain the observed isolated deterioration of SP latencies that might follow retinotopic deficits in the hemifield contralateral to the targeted right V5. At the same time initial acceleration (SR task), SP maintenance (TRI task) and top-down aspects of SP in the blanking task (TRIBL task), which would rather indicate directional effects [18], remained unaffected [21]. Retinotopic SP deficits could indicate the involvement of peripheral representations in MT, in contrast to foveal MT representations, and/or adjacent MST parts. Lesions of the latter also result in directional SP deficits [16,17,19]. In contrast to tDCS targeting V5, no SP modulation was observed by tDCS targeting right FEF, further marking the spatial specificity of personalized tDCS targeting right V5. We conclude that in our experiment personalized cathodal tDCS specifically modulated early sensorimotor transformation within V5 putative subregion MT, or feedforward communication from MT to MST. We further speculate, either that sensorimotor transformation of foveated visual motion information was not affected by personalized cathodal tDCS, or that tDCS-induced initial directional disturbances were compensated by higher-order cognitive mechanisms coming into play under maintenance of ongoing SP [28,29,70–72].

317 **3.2 Personalized cathodal tDCS targeting V5 transiently reduces cortical excitability**

318 Conventionally, cathodal tDCS has been defined as placing the cathode (anode) over the
319 assumed target region to reduce (increase) cortical excitability [73]. Among other mechanistic
320 explanations for tDCS [74], it has been proposed that tDCS electric fields induce cortical
321 membrane polarizations that lead to a subthreshold modulation of neuronal firing-rates and
322 altered cortical excitability [73,75], in addition to changes of blood flow [76] and local
323 GABA/glutamate metabolism at the stimulation site [77–79]. Cathodal tDCS specifically was
324 described to reduce cortical excitability [73,75] and local glutamate concentration [78].
325 Therefore, personalized cathodal tDCS in the present study presumably reduced cortical
326 excitability in V5, thereby hampering the integration of visual motion information to elicit SP
327 initiation as indicated by delayed SP latencies.

328 We observed a transient modulation of SP latencies by single-bout personalized
329 cathodal tDCS (online-effect). No after-effects were observed 15 minutes after tDCS or
330 thereafter. Instead, the online tDCS effect on SP initiation evolved slowly over the 20 minutes
331 tDCS resulting in a significant latency difference between the first (t_{TDCS_5}) and the last (t_{TDCS_20})
332 read-out timepoints. Immediate tDCS modulations were previously shown to induce NMDA-
333 receptor mediated long-term plasticity (LTP) or long-term depression (LTD) that drive longer-
334 lasting tDCS effects [80–82]. Thus, we conclude that personalized cathodal tDCS in the present
335 study induced immediate changes in MT excitability which exerted a statistically robust tDCS
336 effect on behavioral SP performance only when tDCS-induced LTD-like effects were
337 established after several minutes of continuous tDCS.

338 In previous studies, both anodal and cathodal tDCS over V5 induced an improvement in
339 the discrimination accuracy of coherent motion perception in visual scenes [40]. Following
340 previous speculations [37], Battaglini and colleagues [40] suggested that, on the one hand,

341 anodal tDCS increases coherent motion discrimination by increasing the excitability of
342 neurons in the putative subregion MT of V5 that are tuned to correlated motion signals. On
343 the other hand, cathodal tDCS reduces the overall excitability of MT, thereby relatively
344 reducing the response to uncorrelated noise in competing motion scenes with low coherence.
345 At the same time, cathodal tDCS also reduces the discrimination of coherent motion signals in
346 visual scenes with high signal-to-noise ratio. In line with this evidence, we observed a specific
347 impairment of the direct and naturalistic SP sensorimotor response to a single moving visual
348 target without competing motion noise (i.e., with high signal-to-noise ratio) during
349 personalized cathodal tDCS. We further speculate that we did not observe performance
350 facilitation by personalized anodal tDCS in the present young, healthy participants due to a
351 ceiling effect [83] of their anyway high SP performance, in addition to practice-associated
352 improvements obtained during the study (Supplement) [27]. In contrast, impaired SP latencies
353 observed in the elderly and clinical populations [28–30], might be improved by anodal tDCS
354 representing interesting target populations to further examine the clinical benefits of
355 (personalized) tDCS for future studies.

356 Taken together, by applying personalized, i.e., targeted tDCS and differentiating distinct
357 functional properties of SP, we can pinpoint the modulation of SP latencies by personalized
358 cathodal tDCS to an early phase of sensorimotor transformation, presumably involving
359 reduced excitability and LTD-like modulation of V5 subregion MT that delays SP performance.
360

361 **3.3 Normative tDCS over V5 does not modulate pursuit initiation**

362 In contrast to the specific modulation of ipsiversive SP latencies during personalized
363 tDCS targeting V5, no online effect was observed by normative tDCS over V5, extending
364 previous findings [30] that normative tDCS over V5 did not result in any tDCS after-effects on

365 SP [27]. However, simulations of tDCS electric fields in a small sample (N = 6) already suggested
366 rather small target directionalities by normative tDCS that could be increased by personalized
367 tDCS montages with respect to individual targets. Here, we confirm, in a much larger sample,
368 that normative tDCS over V5 yields limited target directionalities, compared to personalized
369 tDCS targeting V5. This improvement of simulated personalized compared to normative
370 electric fields is in line with previous findings of increased personalized directionalities when
371 targeting the parietal cortex [60], the somatosensory cortex [61] and increased electric fields
372 across the brain and within the target region for personalized electric fields targeting the
373 auditory cortex [63]. Furthermore, we extend previous findings by whole-brain analysis of
374 personalized compared to normative simulated electric fields indicating reduced spatial
375 extent of the targeted electric fields and a shift of the electric field topography away from
376 bilateral non-target parietal regions and towards individual target V5 estimates in temporal
377 regions within the right hemisphere (Fig. 2E-F).

378 Although it has been proposed repeatedly to implement electric field simulations and
379 optimization in tES protocols [48,56–58,84], actual applications of personalized tES remain
380 rare [53,61–63]. Thus, little is known about the gain of personalized, compared to
381 conventional normative tES. Therefore, in addition to the analysis of simulated electric fields,
382 we investigated whether the observed behavioral online effect of personalized cathodal tDCS
383 on ipsiversive SP latencies were specific to the applied personalization approach, by re-
384 analyzing data from a matched sample where normative tDCS was applied over the right V5.
385 In contrast to personalized tDCS targeting V5, we did not observe a modulation of SP during
386 normative tDCS over V5. A more detailed analysis indicated a significantly increased tDCS
387 effect on SP by personalized cathodal tDCS, compared to normative cathodal tDCS. We thus
388 follow that the increased theoretical efficacy of personalized compared to normative tDCS of

389 V5 as indicated by electric field simulations holds true for the actual modulation of SP latencies
390 as direct behavioral read-out of the tDCS-effect. Only a few previous studies provided data
391 from applied personalized tDCS [61] or tACS [53,62,63] and only two of those provided a direct
392 comparison of personalized versus normative tES [61,63]. To our knowledge, as of now, no
393 study described the gain by personalized compared to normative tDCS with respect to the
394 modulation of behavior. Khan and colleagues [61] found a significant modulation of
395 somatosensory evoked activity by personalized tDCS targeting the primary somatosensory
396 cortex in ten subjects, but no effect by normative tDCS. In the same study, personalized
397 transcranial electric fields optimized with the DCMI algorithm [85] reached simulated target
398 directionalities of 0.38 ± 0.21 V/m, compared to 0.26 ± 0.13 V/m for normative tDCS (2 mA).
399 In line with these results, our present data indicate that personalized tDCS using the DCMI
400 algorithm targeting V5 shifts the electric field topography towards the explicitly defined tDCS
401 target and thereby increases target directionalities above the effective threshold at the group-
402 level. Normative tDCS may not produce reliable results, due to the relatively limited and
403 untargeted electric fields. Especially in the light of a growing interest in tDCS for clinical
404 application [86,87], our present findings support the huge potential of personalized tES
405 approaches directing individual transcranial electric fields to the assumed cortical target,
406 thereby maximizing the individual stimulation efficacy.

407 In another study, the application of 2 Hz tACS targeting the auditory cortex (stimulation
408 intensity: ±0.5 mA) induced a phase-specific modulation of frequency-modulated sounds by
409 personalized tACS, but also for normative tACS [63]. In this light, it must be noted that
410 personalized tES does not necessarily increase effectiveness, compared to normative tES.
411 Indeed, normative tES can greatly reduce the resources required for experimental and clinical
412 applications considering additional data acquisition and analysis for target localization,

413 individual head models, and electrode positions needed for the optimization and careful
414 application of personalized tES [48]. To conclude, we suggest that personalized and normative
415 approaches should be handled complementary: By specific assumptions about the individual
416 anatomy and the individual functional tES targets, personalized tES is predestined to test
417 hypotheses about the functional mechanisms underlying specific tES applications, for example
418 the role of V5 in the modulation of SP, as shown in the present study. Naturally, personalized
419 tES combines the analysis of tES read-out parameters with simulated electric fields and
420 neurophysiological data that can inform and extend the analysis. These insights can then be
421 used to validate implicit assumptions of normative tES applications or to *a priori* inform the
422 optimization of next-generation, resource-efficient and effective normative tES montages, as
423 a complementary approach to data-intensive *a posteriori* optimization of normative tES
424 montages [55,88].
425
426
427 In this study, our main finding shows that personalized cathodal tDCS targeting right V5
428 specifically delayed latencies of ipsiversive SP due to a transient but LTD-like modulation of
429 early sensorimotor transformation in the MT subregion of V5. Personalized tDCS targeting the
430 right FEF as a control region did not modulate pursuit performance indicating the spatial
431 specificity of personalized tDCS targeting V5 and suggest that these effects cannot be
432 explained by the personalization procedure per se. Further, FEM simulations of electric fields
433 suggest that the observed gain of (effective) personalized tDCS, compared to (ineffective)
434 normative tDCS of V5 might be attributed to topographical shifts of personalized transcranial
435 electric fields towards the targeted right V5 at group-level, as well as increased target
436 directionalities and reduced spatial extent. We suggest that personalized tDCS, and tES in

437 general, might be an interesting methodological perspective to increase tES efficacy,
438 especially in clinical research and therapeutical settings.
439

440 ## 4. Materials and methods

441 ### 4.1 Participants and procedure

442 Twenty healthy participants were recruited for the application of personalized tDCS
443 targeting V5 (experiment 1) and FEF (experiment 2), respectively. One participant did not
444 complete the experiment due to personal reasons. Thus, complete datasets of nineteen
445 participants were included in the analyses (Tab. 1). To compare results from personalized tDCS
446 to the application of normative tDCS, a subsample from a previous study applying normative
447 tDCS over V5 [27] was statistically matched to the personalized tDCS sample with respect to
448 age, gender, laterality index, MWT-B percentile ranks and BDI-II raw values (paired *t*-tests, all
449 $p \geq .25$; Tab. 1) and data was re-analyzed. All participants reported no history of psychiatric or
450 neurological disorders and no psychotic disorders of first-degree family members. Participants
451 had normal or corrected-to-normal visual acuity (1 ± 0.1) and gave written informed consent
452 in line with the declaration of Helsinki prior to the experiment. The study was approved by the
453 ethics committees of the Universities of Lübeck and Münster (#20-459 and #2015-263-f-S).
454 In a full within-subject design, participants completed a battery of SP tasks during eight
455 experimental sessions (Fig. 1; single-blind, see Supplement). During the first session, structural
456 MRI data was recorded to compute individual FEM head models. Additionally, fMRI activity
457 was recorded while subjects [89,90] performed a SP task to localize areas V5 and FEF, in each
458 participant individually. During the second session, combined MEEG was recorded while SP
459 was performed to define the target neuronal orientation at the fMRI-based locations of V5
460 and FEF [89]. In addition, MEEG data was recorded during electrical stimulation of the median

461 nerve to estimate individual skull conductivities based on somatosensory evoked MEEG
462 activity [90] to inform combined MEEG source analysis and target orientation determination.
463 In the following sections, we describe how we used the resulting individually skull-conductivity
464 calibrated FEM head models (section 4.2) to compute personalized tDCS montages for the
465 individual targets in V5 and FEF (section 4.3 and 4.4). Subsequently, sham-controlled
466 personalized anodal and cathodal tDCS targeting areas V5 and FEF was applied in six
467 subsequent experimental sessions (section 4.5; tDCS conditions and target area were pseudo-
468 randomly assigned) to modulate SP performance (section 4.6). In addition, personalized tDCS
469 targeting V5 was compared to normative tDCS over V5, with respect to simulated transcranial
470 electric fields and SP performance under modulation by tDCS (section 4.7). In section 4.8 the
471 statistical analysis is described.
472
473 **4.2 Calibrated individual FEM head models**
474 Structural MRI data were recorded using a 3-T Siemens Magnetom Skyra scanner
475 (Siemens, Germany) and a 64-channel head coil. In addition to T1- and T2-weighted images
476 (T1: 3D MP-RAGE sequence, TR = 2300 ms, TE =3.6 ms, TI = 1100 ms, FA= 8°; T2: spin echo
477 pulse sequence, TR = 3200 ms; TE = 408 ms, FA = 120°; both at 1 x 1 x 1 mm resolution and
478 192 x 256 x 256 mm FoV), DWI data were acquired for 64 direction vectors (turbo spin echo
479 sequence, 69 volumes, 1 x 1 x 1 mm resolution, 100 x 100 x 72 mm FoV, SMS with slice
480 acceleration factor 4, TR = 5500 ms, TE = 128 ms, FA = 90°, b = 1000 s/mm^2) and five additional
481 volumes were acquired with diffusion sensitivity b = 0 s/mm^2.
482 Individual geometry-adapted six-compartment hexahedral FEM head models were
483 computed, including calibrated skull conductivities and white matter conductivity anisotropy
484 [27,91] with the DUNEuro toolbox (see Supplement for details). Conductivities were set to

485 normative values for scalp (0.43 S/m), CSF (1.79 S/m), gray matter (0.33 S/m) and white matter
486 (0.14 S/m). For the EEG lead field, skull conductivities were individually calibrated (skull
487 compacta: 0.013 ± 0.01 S/m, skull spongiosa: 0.0468 ± 0.036 S/m; see Supplement) [90,91].
488 Finally, the EEG lead fields for estimation of the tDCS target orientations, and individual
489 geometry matrices for the tDCS optimization were computed using the calibrated skull
490 conductivities.

491

492 **4.3 Functional localization of V5 and FEF tDCS targets**

493 Personalized tDCS montages were computed based on individual estimates of the
494 stimulation targets in areas V5 (experiment 1) and FEF (experiment 2) of the right hemisphere,
495 respectively (Fig. 1E, Fig. 2) [27], as described in more detail below.

496 First, to determine the target locations of V5 and FEF using fMRI, blood oxygen level
497 dependent (BOLD) activity was recorded (simultaneous multislice (SMS) with acceleration
498 factor 4, 307 Volumes, TR = 980 ms, TE = 30 ms, FA = 70°, resolution 3 x 3 x 3 mm, 68 x 68 x 56
499 mm) while participants performed SP (red dot as SP target, diameter 0.5°, black background;
500 1920 x 1080 screen resolution, 60 Hz refresh rate, NordicNeuroLab, Norway) and eye
501 movements were recorded (Eyelink 1000Plus, 1000 Hz sampling rate; SR Research Ltd.,
502 Canada). Participants completed a test battery of SP-tasks similar to the tasks during the tDCS
503 experiments (see Supplement). Each pursuit block was preceded by fixation intervals with a
504 centrally presented red dot (12 s, diameter 0.5°). Functional images were slice-timing
505 corrected, smoothed (6 mm FWHM Gaussian kernel), and co-registered to the normalized T1
506 image. Individual locations of visual area V5 and FEF in the right hemisphere were determined
507 as local maxima of BOLD activity during SP near putative V5 and FEF regions (Tab. S1) [7,64] in
508 contrast to fixation intervals (*t*-test, $p < .05$ across 5 adjacent voxels, FWE-corrected).

509 Second, individual target orientations were estimated using beamforming at the right
510 V5 and FEF target locations defined by functional MRI. Therefore, combined MEEG data were
511 recorded (EEG: 60 channels, Easycap, Germany; MEG: 275 axial gradiometers, VSM MedTech
512 Ltd., Canada; 600 Hz sampling rate) while participants completed a continuous pursuit task
513 (TRI; 18.7°/s, ±15° amplitude, 20 blocks of each 8 ramps to the left and right interleaved with
514 short breaks). Before the first block and after the 10th block, participants fixated a red dot in
515 the center of the screen for 15 s. Data were filtered (0.1 Hz highpass-filter, 50 Hz notch filter
516 considering harmonics), cut into 320 epochs (0 to 1.59 s length relative to ramp onsets to left
517 and right), and demeaned. Invalid epochs were rejected semi-automatically (rejected trials:
518 15.3 ± 11.3 %) and the EEG data was re-referenced to the average reference. tDCS target
519 orientations were estimated using linearly constrained minimum variance (LCMV)
520 beamforming with Unit-Noise-Gain constraint (regularization parameter $\lambda = 5\%$), following the
521 procedure described in [89] (see Supplement for details).

522 Electrode positions for the tDCS montage optimization were recorded (FASTRAK,
523 Polhemus Inc., VT/USA). These 74 electrode positions follow the 10-20-system, embedded in
524 a standard EEG cap layout (Easycap, Germany), of which 60 electrodes were used as EEG
525 sensors.

526

527 **4.4 Computation of personalized tDCS montages and electric field simulations**

528 Based on individual anatomical information, integrated in the head models and
529 individual target information from the localizer tasks, personalized tDCS montages were
530 computed to target the area V5 (experiment 1) or FEF (experiment 2), respectively. To this
531 end, the distributed constrained maximum intensity (DCMI) algorithm [53,60,61,85] was
532 employed to compute the personalized tDCS montage that maximizes the injected current at

533 the target location along the target orientation (i.e., the directionality; see Supplement for
534 details). Resulting montages described personalized cathodal tDCS montages. Herein, we
535 define the applied personalized tDCS montages relative to the estimated target orientations,
536 i.e., personalized cathodal tDCS results in montages with the cathodes placed on the scalp
537 roughly in the direction of the estimated target orientation. For personalized anodal tDCS, the
538 polarity of each electrode was inverted. This definition does not resemble normative tDCS
539 conventions where the cathodes/anodes are placed on the scalp directly over the proposed
540 target location defining cathodal/anodal tDCS. This convention implicitly assumes quasi-radial
541 targets but does not consider tangential targets or inter-individual target localization
542 variability. The target orientations in the present study were estimated as the MEEG summed
543 dipole orientation that might not directly reflect the local cortical structure, but rather
544 functional properties of the target orientation. Therefore, the definition of personalized
545 cathodal/anodal tDCS considers individual target locations and orientations.

546

547 **4.5 Application of personalized tDCS**

548 During tDCS (t_{TDCS}) personalized anodal, cathodal, or sham tDCS was applied targeting
549 the right V5 and FEF in six pseudo-randomized sessions, separated by at least four days (7.9 ±
550 7.8 days, M ± SD; Fig. 1C). During each session, 20 minutes of tDCS was applied using a Starstim
551 8 device (Neuroelectrics, Spain). Small Ag/AgCl electrodes (NG Pistim, 3.14 cm^2 surface) were
552 placed in custom empty EEG caps (EasyCap, Germany) with the same layout and cap size as
553 used for the EEG measurement and electrode registration to ensure an accurate placement of
554 the stimulation electrodes according to the optimized personalized montages (Fig. 1E). During
555 personalized anodal and cathodal tDCS, a total of 2 mA current was applied (10 s ramp-on and
556 ramp-off). Sham tDCS was applied by the same montages as used for anodal stimulation, but

557 tDCS was applied for only 30 s in addition to the current ramps.

558 To minimize transcutaneous side-effects, anesthetic creme (2.5 % lidocaine, 2.5 %
559 prilocaine, Anesderm®, Pierre Fabre, Germany) was used [92]. After each t_{TDCS} interval,
560 participants completed a questionnaire asking for their subjectively perceived transcutaneous
561 side-effects during t_{TDCS} (itching, warmth, stitching, throbbing, and pain) on a five-point scale
562 (0 = absent, weak, moderate, pronounced, 4 = intense) [93]. Furthermore, participants rated
563 subjective fatigue for four timepoints during t_{TDCS} on a five-point scale (1 = very alert, awake,
564 moderate, tired, 5 = very tired).

565

566 **4.6 Eye tracking and analysis of eye movement data**

567 During the six tDCS sessions, participants were seated 65 cm in front of an LCD monitor
568 in a closed room with lights off and completed three SP tasks to assess different aspects of SP
569 initiation and maintenance (see Supplement for details) [27]. In short, eye movements were
570 recorded using a video-based eye tracker (Eyelink 1000Plus, SR Research Ltd., Canada). During
571 all tasks, participants were instructed to follow a horizontally moving SP target on the monitor
572 as precisely as possible (red dot with 0.5° diameter, black background; Fig. 1B). During the first
573 task, eight horizontal constant velocity ramps were presented as continuous triangular
574 waveform stimulus (TRI, 18.7°/s, ± 15° amplitude; Fig. 1B-C, Supplement). In the second task,
575 12 similar horizontal velocity ramps were presented with target blanking between 300 to 1000
576 ms relative to ramp onset (18.7°/s, ± 15° amplitude, triangular waveform stimulus with
577 blanking, TRIBL; Fig. 1B-C, Supplement). To specifically assess SP initiation and early SP
578 maintenance eight horizontal foveopetal step-ramp stimuli (SR) were presented [94], pseudo-
579 randomly directed either to the left or the right side of the screen. Step-ramps started with a
580 2.5° step which was immediately followed by a velocity ramp in the opposite direction

581 (18.7°/s, ± 15° amplitude; Fig. 1B-D). To minimize expectation effects, two of eight step-ramps
582 were presented with alternating velocities (9.7 °/s, ± 1.3 ° step-size; 26.7 °/s, ± 3.5 ° step-size).
583 The three tasks were presented in mixed blocks [33] including three task repetitions during
584 each block. This resulted in 24 continuous ramps (TRI), 36 ramps with blanking (TRIBL) and 24
585 step-ramps (SR) per block.

586 Effects of tDCS on SP were assessed by presenting each one block of SP tasks before (t_0),
587 and 15 and 40 minutes after (t_{15}, t_{40}; after-effects) tDCS application in each of the six
588 experimental sessions. Online effects of tDCS were assessed by presenting four repetitions of
589 SP task blocks equally distributed across the 20 minutes tDCS application (t_{TDCS}; i.e., within the
590 first 5, 10, 15, or 20 minutes of tDCS, t_{TDCS_5}, t_{TDCS_10}, t_{TDCS_15}, t_{TDCS_20}; Fig. 1C). During t_{TDCS}, SP
591 task blocks were separated by simple oculomotor tasks to activate the oculomotor system
592 during the stimulation, while providing an active rest for the participants at the same time.
593 Overall, this resulted in 504 continuous ramps (TRI), 756 ramps with blanking (TRIBL) and 504
594 step-ramps (SR) that were analyzed for each subject during experiment 1 (V5) and experiment
595 2 (FEF), respectively.

596 SP data analysis focused on SP velocity, computed as the first derivative of eye position.
597 Continuous data were epoched (-100 to 1600 ms for TRI and TRIBL and -100 to 1300 ms for SR
598 relative to the ramp onset) and invalid epochs were rejected (experiment 1 (V5): 1.5 ± 2.1 %
599 epochs were rejected; see Supplement). Median eye velocity across epochs was computed
600 separately for each subject, tDCS condition (anodal, cathodal, sham), timepoint (t_0, t_{TDCS_5},
601 t_{TDCS_10}, t_{TDCS_15}, t_{TDCS_20}, t_{15}, t_{40}) and stimulus direction (leftward, rightward). SP velocity
602 parameters were computed to assess different aspects of SP performance during SP initiation
603 (SR: SP latency, initial eye acceleration; Fig. 1D) as well as ongoing SP (SR: early maintenance
604 gain; TRI: maintenance gain, gain = eye velocity/target velocity; TRIBL: preblank, residual and

605 postblank velocity gains, deceleration and deceleration latency at the start of the blanking
606 interval, as well as re-acceleration and re-acceleration latency at the end of the blanking
607 interval) [27,71].
608
609 **4.7 Comparing personalized tDCS targeting V5 and normative tDCS over V5**
610 Results from personalized tDCS targeting V5 (experiment 1) were compared to results
611 from the application of normative tDCS over V5 (experiment 3; Tab. 1). The normative
612 application of V5 was designed identically to the personalized procedure with respect to the
613 SP test battery and the overall application of tDCS [27] and data from experiment 3 was re-
614 analyzed according to the analysis procedure in experiment 1. However, instead of
615 personalized tDCS montages, normative tDCS montages were used in experiment 3 that did
616 not vary across subjects, thus also no MEEG and MRI data were acquired before the normative
617 tDCS experiment. In short, to apply normative tDCS, two stimulation electrodes were placed
618 over area V5 of the right hemisphere (PO8, P8) with two central return electrodes (Cp1, Cz)
619 [36,37] according to the 10-20 system. During normative tDCS, 2 mA current was applied for
620 20 minutes, restricted to 1 mA per electrode. Eye movements were recorded during the same
621 timepoints as in the personalized experiment (t_0, t_{TDCS_5}, t_{TDCS_10}, t_{TDCS_15}, t_{TDCS_20}, t_{15}, t_{40}). Since
622 SP during t_{TDCS} were not analyzed in detail by Radecke et al. [27], the data from the matched
623 sample were re-analyzed for all tDCS timepoints (t_{TDCS_5}, t_{TDCS_10}, t_{TDCS_15}, t_{TDCS_20}) to compare
624 online effects on the SP performance by normative versus personalized tDCS.
625 Furthermore, electric field simulations were compared between normative and
626 personalized montages to estimate the differences in the potential efficacy between the two
627 tDCS methods, given the individual estimates of the V5 tDCS target. Therefore, normative
628 electric field simulations were computed for the N = 19 subjects from the personalized tDCS

629 sample, using the normative electrode placement, since data for these participants for
630 computation of individual head models and estimation of individual tDCS targets were
631 available. To quantify individual transcranial electric field parameters (see Supplement for
632 details), for each subject, we computed the target intensity ($|E|_{IT}$) the target intensity
633 corrected for the parallelity between the stimulation target orientation vector and the target
634 electric field orientation vector (directionality, $|E|_{DIR}$) [53,60,61], as well as the spatial extent
635 of the electric field relative to the stimulation target ($|E|_{EXTENT}$) [53,60]. The overall cortical
636 electric field ($|\mathbf{E}|$) and electric field parameters with respect to the individual stimulation
637 targets ($|E|_{IT}$, $|E|_{DIR}$, $|E|_{EXTENT}$) were compared between personalized versus normative tDCS.
638 For illustration, individual electric fields were interpolated on a common MNI cortical grid and
639 averaged across subjects (Fig. 2).
640
641 **4.8 Statistical analysis of tDCS effects**
642 To analyze tDCS effects on SP performance, linear mixed models (LMMs) were fitted to
643 the data (IBM SPSS Statistics, IBM Corp., USA) for each estimated SP parameter and separately
644 for experiment 1 (V5-personalized), experiment 2 (FEF-personalized), and experiment 3 (V5-
645 normative). In a full within-subject design, tDCS condition (anodal, cathodal, sham), timepoint
646 (t_0, t_{TDCS_5}, t_{TDCS_10}, t_{TDCS_15}, t_{TDCS_20}, t_{15}, t_{40}) and the visual stimulus direction (leftward,
647 rightward) were included as fixed effect factors. To control inter-individual variability of SP
648 performance, subject ID was included as random effects factor (random intercept; identity
649 covariance structure). tDCS condition, timepoint and ramp direction were considered as
650 repeated factors (first-order autoregressive covariance structure). Main and interaction
651 effects were analyzed in a saturated model. In case of specific tDCS effects (i.e., an interaction
652 between tDCS condition, timepoint, and ramp direction), separate LMM analyses were

computed for timepoints of online effects (t_{TDCS_5}, t_{TDCS_10}, t_{TDCS_15}, t_{TDCS_20}) and (after-)effects relative to t_0 (t_0, t_{TDCS}, t_{15}, t_{40}, using the averaged performance across all t_{TDCS} timepoints), further including tDCS condition and ramp direction as factors.

The significance level was set to α = .05 and post-hoc contrasts of estimated marginal means were computed for the highest-order interaction or main effect (Bonferroni-corrected for multiple comparisons). *F*-values and *p*-values are reported for significant main or interaction effects. For post-hoc tests, Bonferroni-corrected *p*-values, mean and standard error of the mean are reported. Effect sizes were estimated as the absolute value of Cohen's $d_z = \frac{t}{\sqrt{N}}$ with *N* being the respective sample size and *t* being the *t*-value computed based on the mean difference and standard error of the mean of the difference between estimated marginal means of the respective paired post-hoc contrast [95].

Furthermore, significant LMM tDCS condition * timepoint * stimulus direction interactions indicate specific tDCS effects. To follow-up these results in more detail, tDCS online effects were defined as the difference between the first and the last timepoint during t_{TDCS} (t_{TDCS_20} - t_{TDCS_5}) of the respective SP parameter, irrespective of the temporal evolution of this effect. A second, complementary estimate of tDCS effects was computed as the slope (*b*) of a robust linear regression computed across all timepoints during t_{TDCS} (t_{TDCS_5} to t_{TDCS_20}) assuming a quasi-linear evolution of the tDCS effect during the stimulation (Fig. 3). Both tDCS effect measures were compared between stimulus directions for each tDCS condition, as well as between tDCS conditions for each stimulus direction using bootstrapped paired *t*-tests (*n* = 10000 bootstrap samples were computed to determine the H_0 distribution). In addition, tDCS effects for the respective tDCS condition and stimulus direction were compared across experiments using bootstrapped paired *t*-tests to compare between experiment 1 (V5-personalized) versus experiment 2 (FEF-personalized) and unpaired *t*-tests to compare

experiment 1 (V5-personalized) versus experiment 3 (V5-normative). For all bootstrap *t*-tests *z*-values and *p*-values (Bonferroni-corrected) are reported and Cohens d_z (paired contrast) or d_s (unpaired contrast) was computed based on the observed values [95].

Electric field simulations were compared between normative versus personalized tDCS montages. Individually simulated electric fields were interpolated on an MNI cortical surface representation and paired *t*-tests were computed for every position of the surface grid between personalized and normative tDCS (FDR-corrected) [96]. Furthermore, separate bootstrap paired *t*-test were computed (one-sided) with 10000 iterations using MATLAB (The Mathworks Ltd., MA/USA) for $|E|_{IT}$, $|E|_{DIR}$, and $|E|_{EXTENT}$. For each test, *z*-value, *p*-value and descriptive means and standard errors of the means are reported. Effect size d_z was estimated based on the observed values [95].

CRediT authorship contribution statement

Jan-Ole Radecke: Conceptualization, Methodology, Software, Investigation, Formal analysis, Writing - original draft, Visualization. **Alexander Kühn:** Investigation, Data curation, Formal Analysis, Writing – review & editing. **Tim Erdbrügger and Yvonne Buschermöhle:** Investigation, Methodology, Software, Writing - review & editing. **Sogand Rashidi and Hannah Stöckler:** Investigation, Data curation, Writing – review & editing. **Benjamin Sack:** Investigation, Writing - review & editing. **Stefan Borgwardt:** Resources, Supervision, Writing - review & editing. **Till R. Schneider:** Supervision, Methodology, Writing - review & editing. **Joachim Gross:** Supervision, Funding acquisition, Writing - review & editing. **Carsten H. Wolters:** Supervision, Project administration, Funding acquisition, Writing - review & editing. **Andreas Sprenger:** Methodology, Software, Supervision, Writing – review & editing. **Rebekka Lencer:** Project administration, Funding acquisition, Conceptualization, Writing - review & editing.

Acknowledgements

This work was supported by the German Research Foundation (DFG; WO1425/10-1 to CHW, GR2024/8-1 to JG and LE1122/7-1 to RL) and by the Bundesministerium für Gesundheit (BMG; ZMI1-2521FSB006, under the frame of ERA PerMed as project ERAPERMED2020-227). JG was further supported by the DFG (GR2024/11-1, GR2024/12-1, TRR393). JOR was funded by the Clinician Scientist program of the Section of Medicine of the University of Lübeck. We thank

Dr. Martin Göttlich and Andreas Wollbrink for technical support, Karin Wilken, Hildegard Deitermann, Ute Trompeter, Susanne Schellbach and Mandy-Josephine Reichhardt for support with the data acquisition, and Prof. Peter Trillenberg for helpful discussions.

References

1. Agtzidis I, Meyhöfer I, Dorr M, Lencer R. Following Forrest Gump: Smooth pursuit related brain activation during free movie viewing. Neuroimage. 2020;216: 116491. doi:10.1016/j.neuroimage.2019.116491
2. Lisberger SG. Visual Guidance of Smooth-Pursuit Eye Movements: Sensation, Action, and What Happens in Between. Neuron. 2010;66: 477–491. doi:10.1016/j.neuron.2010.03.027
3. Schutz AC, Braun DI, Gegenfurtner KR. Eye movements and perception: A selective review. J Vis. 2011;11: 9–9. doi:10.1167/11.5.9
4. Lencer R, Trillenberg P. Neurophysiology and neuroanatomy of smooth pursuit in humans. Brain Cogn. 2008;68: 219–228. doi:10.1016/j.bandc.2008.08.013
5. Ilg UJ, Thier P. The neural basis of smooth pursuit eye movements in the rhesus monkey brain. Brain Cogn. 2008;68: 229–240. doi:10.1016/j.bandc.2008.08.014
6. Wilms M, Eickhoff SB, Specht K, Amunts K, Shah NJ, Malikovic A, et al. Human V5/MT+: comparison of functional and cytoarchitectonic data. Anat Embryol (Berl). 2005;210: 485–495. doi:10.1007/s00429-005-0064-y
7. Ohlendorf S, Sprenger A, Speck O, Glauche V, Haller S, Kimmig H. Visual motion, eye motion, and relative motion: A parametric fMRI study of functional specializations of smooth pursuit eye movement network areas. J Vis. 2010;10: 21–21. doi:10.1167/10.14.21
8. Dukelow SP, DeSouza JFX, Culham JC, van den Berg A V., Menon RS, Vilis T. Distinguishing Subregions of the Human MT+ Complex Using Visual Fields and Pursuit Eye Movements. J Neurophysiol. 2001;86: 1991–2000. doi:10.1152/jn.2001.86.4.1991
9. Komatsu H, Wurtz RH. Relation of cortical areas MT and MST to pursuit eye movements. I. Localization and visual properties of neurons. J Neurophysiol. 1988;60: 580–603. doi:10.1152/jn.1988.60.2.580
10. Komatsu H, Wurtz RH. Modulation of pursuit eye movements by stimulation of cortical areas MT and MST. J Neurophysiol. 1989;62: 31–47. doi:10.1152/jn.1989.62.1.31
11. Newsome WT, Wurtz RH, Komatsu H. Relation of cortical areas MT and MST to pursuit eye movements. II. Differentiation of retinal from extraretinal inputs. J Neurophysiol. 1988;60: 604–620. doi:10.1152/jn.1988.60.2.604
12. Lee J, Joshua M, Medina JF, Lisberger SG. Signal, Noise, and Variation in Neural and Sensory-Motor Latency. Neuron. 2016;90: 165–176. doi:10.1016/j.neuron.2016.02.012
13. Lee J, Darlington TR, Lisberger SG. The Neural Basis for Response Latency in a Sensory-Motor Behavior. Cerebral Cortex. 2020;30: 3055–3073. doi:10.1093/cercor/bhz294
14. Ferrera VP. Smooth pursuit preparation modulates neuronal responses in visual areas MT and MST. J Neurophysiol. 2015;114: 638–649. doi:10.1152/jn.00636.2014
15. Lee J, Lisberger SG. Gamma Synchrony Predicts Neuron–Neuron Correlations and Correlations with Motor Behavior in Extrastriate Visual Area MT. The Journal of Neuroscience. 2013;33: 19677–19688. doi:10.1523/JNEUROSCI.3478-13.2013
16. Newsome W, Wurtz R, Dursteler M, Mikami A. Deficits in visual motion processing following ibotenic acid lesions of the middle temporal visual area of the macaque monkey. The Journal of Neuroscience. 1985;5: 825–840. doi:10.1523/JNEUROSCI.05-03-00825.1985
17. Newsome W, Wurtz R. Probing visual cortical function with discrete chemical lesions. Trends Neurosci. 1988;11: 394–400. doi:10.1016/0166-2236(88)90076-8
18. Dursteler MR, Wurtz RH. Pursuit and optokinetic deficits following chemical lesions of cortical areas MT and MST. J Neurophysiol. 1988;60: 940–965. doi:10.1152/jn.1988.60.3.940
19. Dursteler MR, Wurtz RH, Newsome WT. Directional pursuit deficits following lesions of the foveal representation within the superior temporal sulcus of the macaque monkey. J Neurophysiol. 1987;57: 1262–1287. doi:10.1152/jn.1987.57.5.1262
20. Heide W, Kurzidim K, Kömpf D. Deficits of smooth pursuit eye movements after frontal and parietal lesions. Brain. 1996;119: 1951–1969. doi:10.1093/brain/119.6.1951
21. Sharpe JA. Neurophysiology and neuroanatomy of smooth pursuit: Lesion studies. Brain Cogn. 2008;68: 241–254. doi:10.1016/j.bandc.2008.08.015

22. Thurston SE, Leigh RJ, Crawford T, Thompson A, Kennard C. Two distinct deficits of visual tracking caused by unilateral lesions of cerebral cortex in humans. Ann Neurol. 1988;23: 266–273. doi:10.1002/ana.410230309
23. Haarmeier T, Kammer T. Effect of TMS on Oculomotor Behavior but not Perceptual Stability during Smooth Pursuit Eye Movements. Cerebral Cortex. 2010;20: 2234–2243. doi:10.1093/cercor/bhp285
24. Nagel M, Sprenger A, Hohagen F, Binkofski F, Lencer R. Cortical mechanisms of retinal and extraretinal smooth pursuit eye movements to different target velocities. Neuroimage. 2008;41: 483–492. doi:10.1016/j.neuroimage.2008.02.058
25. Nagel M, Sprenger A, Steinlechner S, Binkofski F, Lencer R. Altered Velocity Processing in Schizophrenia during Pursuit Eye Tracking. Lappe M, editor. PLoS One. 2012;7: e38494. doi:10.1371/journal.pone.0038494
26. Lencer R, Nagel M, Sprenger A, Heide W, Binkofski F. Reduced neuronal activity in the V5 complex underlies smooth-pursuit deficit in schizophrenia: evidence from an fMRI study. Neuroimage. 2005;24: 1256–1259. doi:10.1016/j.neuroimage.2004.11.013
27. Radecke J-O, Sprenger A, Stöckler H, Espeter L, Reichhardt M-J, Thomann LS, et al. Normative tDCS over V5 and FEF reveals practice-induced modulation of extraretinal smooth pursuit mechanisms, but no specific stimulation effect. Sci Rep. 2023;13: 21380. doi:10.1038/s41598-023-48313-z
28. Sprenger A, Trillenberg P, Pohlmann J, Herold K, Lencer R, Helmchen C. The role of prediction and anticipation on age-related effects on smooth pursuit eye movements. Ann N Y Acad Sci. 2011;1233: 168–176. doi:10.1111/j.1749-6632.2011.06114.x
29. Helmchen C, Pohlmann J, Trillenberg P, Lencer R, Graf J, Sprenger A. Role of anticipation and prediction in smooth pursuit eye movement control in Parkinson's disease. Movement Disorders. 2012;27: 1012–1018. doi:10.1002/mds.25042
30. Knox PC, Davidson JH, Anderson D. Age-related changes in smooth pursuit initiation. Exp Brain Res. 2005;165: 1–7. doi:10.1007/s00221-005-2265-2
31. Campion D, Thibaut F, Denise P, Courtin P, Pottier M, Levillain D. SPEM impairment in drug-naive schizophrenic patients: Evidence for a trait marker. Biol Psychiatry. 1992;32: 891–902. doi:10.1016/0006-3223(92)90178-3
32. Lencer R, Malchow CP, Krecker K, Nolte A, Pinnow M, Zimmerman v. Siefart S, et al. Smooth pursuit performance in families with multiple occurrence of schizophrenia and nonpsychotic families. Biol Psychiatry. 1999;45: 694–703. doi:10.1016/S0006-3223(98)00310-2
33. Lencer R, Sprenger A, Reilly JL, McDowell JE, Rubin LH, Badner JA, et al. Pursuit eye movements as an intermediate phenotype across psychotic disorders: Evidence from the B-SNIP study. Schizophr Res. 2015;169: 326–333. doi:10.1016/j.schres.2015.09.032
34. Meyhoefer I, Sprenger A, Derad D, Grotegerd D, Leenings R, Leehr EJ, et al. Evidence from comprehensive independent validation studies for smooth pursuit dysfunction as a sensorimotor biomarker for psychosis. Sci Rep. 2024;14: 13859. doi:10.1038/s41598-024-64487-6
35. Kar K, Krekelberg B. Transcranial Alternating Current Stimulation Attenuates Visual Motion Adaptation. Journal of Neuroscience. 2014;34: 7334–7340. doi:10.1523/JNEUROSCI.5248-13.2014
36. Antal A, Nitsche MA, Kincses TZ, Kruse W, Hoffmann K-P, Paulus W. Facilitation of visuo-motor learning by transcranial direct current stimulation of the motor and extrastriate visual areas in humans. European Journal of Neuroscience. 2004;19: 2888–2892. doi:10.1111/j.1460-9568.2004.03367.x
37. Antal A, Nitsche MA, Kruse W, Kincses TZ, Hoffmann K-P, Paulus W. Direct Current Stimulation over V5 Enhances Visuomotor Coordination by Improving Motion Perception in Humans. J Cogn Neurosci. 2004;16: 521–527. doi:10.1162/089892904323057263
38. Antal A, Edina Varga CT, Nitsche MA, Chadaide Z, Paulus W, Kova G, et al. Direct current stimulation over MT + /V5 modulates motion aftereffect in humans. Neuroreport. 2004;15: 2491–2494.
39. Antal A, Kovács G, Chaieb L, Cziraki C, Paulus W, Greenlee MW. Cathodal stimulation of human MT+ leads to elevated fMRI signal: A tDCS-fMRI study. Restor Neurol Neurosci. 2012;30: 255–263. doi:10.3233/RNN-2012-110208
40. Battaglini L, Noventa S, Casco C. Anodal and cathodal electrical stimulation over V5 improves motion perception by signal enhancement and noise reduction. Brain Stimul. 2017;10: 773–779. doi:10.1016/j.brs.2017.04.128
41. Wiethoff S, Hamada M, Rothwell JC. Variability in response to transcranial direct current stimulation of the motor cortex. Brain Stimul. 2014;7: 468–475. doi:10.1016/j.brs.2014.02.003
42. Tremblay S, Larochelle-Brunet F, Lafleur L, El Mouderrib S, Lepage J, Théoret H. Systematic assessment of duration and intensity of anodal transcranial direct current stimulation on primary motor cortex

excitability. Thut G, editor. European Journal of Neuroscience. 2016;44: 2184–2190. doi:10.1111/ejn.13321
43. López-Alonso V, Cheeran B, Río-Rodríguez D, Fernández-Del-Olmo M. Inter-individual variability in response to non-invasive brain stimulation paradigms. Brain Stimul. 2014;7: 372–380. doi:10.1016/j.brs.2014.02.004
44. Dedoncker J, Brunoni AR, Baeken C, Vanderhasselt M-A. A Systematic Review and Meta-Analysis of the Effects of Transcranial Direct Current Stimulation (tDCS) Over the Dorsolateral Prefrontal Cortex in Healthy and Neuropsychiatric Samples: Influence of Stimulation Parameters. Brain Stimul. 2016;9: 501–517. doi:10.1016/j.brs.2016.04.006
45. Schutter DJLG, Wischnewski M. A meta-analytic study of exogenous oscillatory electric potentials in neuroenhancement. Neuropsychologia. 2016;86: 110–118. doi:10.1016/j.neuropsychologia.2016.04.011
46. Gomez-Tames J, Fernández-Corazza M. Perspectives on Optimized Transcranial Electrical Stimulation Based on Spatial Electric Field Modeling in Humans. J Clin Med. 2024;13: 3084. doi:10.3390/jcm13113084
47. Alekseichuk I, Wischnewski M, Opitz A. A minimum effective dose for (transcranial) alternating current stimulation. Brain Stimul. 2022;15: 1221–1222. doi:10.1016/j.brs.2022.08.018
48. Wischnewski M, Alekseichuk I, Opitz A. Neurocognitive, physiological, and biophysical effects of transcranial alternating current stimulation. Trends Cogn Sci. 2023;27: 189–205. doi:10.1016/j.tics.2022.11.013
49. Esmaeilpour Z, Marangolo P, Hampstead BM, Bestmann S, Galletta E, Knotkova H, et al. Incomplete evidence that increasing current intensity of tDCS boosts outcomes. Brain Stimul. 2018;11: 310–321. doi:10.1016/j.brs.2017.12.002
50. Kasten FH, Duecker K, Maack MC, Meiser A, Herrmann CS. Integrating electric field modeling and neuroimaging to explain inter-individual variability of tACS effects. Nat Commun. 2019;10: 5427. doi:10.1038/s41467-019-13417-6
51. Johnson L, Alekseichuk I, Krieg J, Doyle A, Yu Y, Vitek J, et al. Dose-dependent effects of transcranial alternating current stimulation on spike timing in awake nonhuman primates. Sci Adv. 2020;6: eaaz2747. doi:10.1126/sciadv.aaz2747
52. Antonenko D, Thielscher A, Saturnino GB, Aydin S, Ittermann B, Grittner U, et al. Towards precise brain stimulation: Is electric field simulation related to neuromodulation? Brain Stimul. 2019;12: 1159–1168. doi:10.1016/j.brs.2019.03.072
53. Radecke J-O, Fiene M, Misselhorn J, Herrmann CS, Engel AK, Wolters CH, et al. Personalized alpha-tACS targeting left posterior parietal cortex modulates visuo-spatial attention and posterior evoked EEG activity. Brain Stimul. 2023;16: 1047–1061. doi:10.1016/j.brs.2023.06.013
54. Caulfield KA, Badran BW, DeVries WH, Summers PM, Kofmehl E, Li X, et al. Transcranial electrical stimulation motor threshold can estimate individualized tDCS dosage from reverse-calculation electric-field modeling. Brain Stimul. 2020;13: 961–969. doi:10.1016/j.brs.2020.04.007
55. Wischnewski M, Mantell KE, Opitz A. Identifying regions in prefrontal cortex related to working memory improvement: A novel meta-analytic method using electric field modeling. Neurosci Biobehav Rev. 2021;130: 147–161. doi:10.1016/j.neubiorev.2021.08.017
56. Gross J, Junghöfer M, Wolters CH. Bioelectromagnetism in Human Brain Research: New Applications, New Questions. The Neuroscientist. 2021; 107385842110547. doi:10.1177/10738584211054742
57. Liu A, Vöröslakos M, Kronberg G, Henin S, Krause MR, Huang Y, et al. Immediate neurophysiological effects of transcranial electrical stimulation. Nat Commun. 2018;9. doi:10.1038/s41467-018-07233-7
58. Polanía R, Nitsche MA, Ruff CC. Studying and modifying brain function with non-invasive brain stimulation. Nat Neurosci. 2018;21: 174–187. doi:10.1038/s41593-017-0054-4
59. Evans C, Bachmann C, Lee JSA, Gregoriou E, Ward N, Bestmann S. Dose-controlled tDCS reduces electric field intensity variability at a cortical target site. Brain Stimul. 2020;13: 125–136. doi:10.1016/j.brs.2019.10.004
60. Radecke J-O, Khan A, Engel AK, Wolters CH, Schneider TR. Individual Targeting Increases Control Over Inter-Individual Variability in Simulated Transcranial Electric Fields. IEEE Access. 2020;8: 182610–182624. doi:10.1109/ACCESS.2020.3028618
61. Khan A, Antonakakis M, Suntrup-Krueger S, Lencer R, Nitsche MA, Paulus W, et al. Can individually targeted and optimized multi-channel tDCS outperform standard bipolar tDCS in stimulating the primary somatosensory cortex? Brain Stimul. 2023;16: 1–16. doi:10.1016/j.brs.2022.12.006
62. Mohd Zulkifly MF, Lehr A, van de Velden D, Khan A, Focke NK, Wolters CH, et al. Directionality of the injected current targeting the P20/N20 source determines the efficacy of 140 Hz transcranial alternating current stimulation (tACS)-induced aftereffects in the somatosensory cortex. Schwenkreis P, editor. PLoS One. 2022;17: e0266107. doi:10.1371/journal.pone.0266107

63. Cabral-Calderin Y, van Hinsberg D, Thielscher A, Henry MJ. Behavioral entrainment to rhythmic auditory stimulation can be modulated by tACS depending on the electrical stimulation field properties. Elife. 2024;12. doi:10.7554/eLife.87820
64. Lencer R, Nagel M, Sprenger A, Zapf S, Erdmann C, Heide W, et al. Cortical mechanisms of smooth pursuit eye movements with target blanking. An fMRI study. European Journal of Neuroscience. 2004;19: 1430–1436. doi:10.1111/j.1460-9568.2004.03229.x
65. Tzourio-Mazoyer N, Landeau B, Papathanassiou D, Crivello F, Etard O, Delcroix N, et al. Automated Anatomical Labeling of Activations in SPM Using a Macroscopic Anatomical Parcellation of the MNI MRI Single-Subject Brain. Neuroimage. 2002;15: 273–289. doi:10.1006/nimg.2001.0978
66. Wild B, Treue S. Primate extrastriate cortical area MST: a gateway between sensation and cognition. J Neurophysiol. 2021;125: 1851–1882. doi:10.1152/jn.00384.2020
67. Maunsell J, van Essen D. The connections of the middle temporal visual area (MT) and their relationship to a cortical hierarchy in the macaque monkey. The Journal of Neuroscience. 1983;3: 2563–2586. doi:10.1523/JNEUROSCI.03-12-02563.1983
68. Boussaoud D, Desimone R, Ungerleider LG. Subcortical connections of visual areas MST and FST in macaques. Vis Neurosci. 1992;9: 291–302. doi:10.1017/S0952523800010701
69. Kimmig H, Ohlendorf S, Speck O, Sprenger A, Rutschmann RM, Haller S, et al. fMRI evidence for sensorimotor transformations in human cortex during smooth pursuit eye movements. Neuropsychologia. 2008;46: 2203–2213. doi:10.1016/j.neuropsychologia.2008.02.021
70. Barnes GR. Cognitive processes involved in smooth pursuit eye movements. Brain Cogn. 2008;68: 309–326. doi:10.1016/j.bandc.2008.08.020
71. Trillenberg P, Sprenger A, Talamo S, Herold K, Helmchen C, Verleger R, et al. Visual and non-visual motion information processing during pursuit eye tracking in schizophrenia and bipolar disorder. Eur Arch Psychiatry Clin Neurosci. 2017;267: 225–235. doi:10.1007/s00406-016-0671-z
72. Becker W, Fuchs AF. Prediction in the oculomotor system: smooth pursuit during transient disappearance of a visual target. Exp Brain Res. 1985;57: 562–575. doi:10.1007/BF00237843
73. Nitsche MA, Paulus W. Excitability changes induced in the human motor cortex by weak transcranial direct current stimulation. J Physiol. 2000;527: 633–639. doi:10.1111/j.1469-7793.2000.t01-1-00633.x
74. Krause MR, Zanos TP, Csorba BA, Pilly PK, Choe J, Phillips ME, et al. Transcranial Direct Current Stimulation Facilitates Associative Learning and Alters Functional Connectivity in the Primate Brain. Current Biology. 2017;27: 3086-3096.e3. doi:10.1016/j.cub.2017.09.020
75. Creutzfeldt OD, Fromm GH, Kapp H. Influence of transcortical d-c currents on cortical neuronal activity. Exp Neurol. 1962;5: 436–452. doi:10.1016/0014-4886(62)90056-0
76. Jamil A, Batsikadze G, Kuo H, Meesen RLJ, Dechent P, Paulus W, et al. Current intensity- and polarity-specific online and aftereffects of transcranial direct current stimulation: An fMRI study. Hum Brain Mapp. 2020;41: 1644–1666. doi:10.1002/hbm.24901
77. Bachtiar V, Near J, Johansen-Berg H, Stagg CJ. Modulation of GABA and resting state functional connectivity by transcranial direct current stimulation. Elife. 2015;4. doi:10.7554/eLife.08789
78. Stagg CJ, Best JG, Stephenson MC, O'Shea J, Wylezinska M, Kincses ZT, et al. Polarity-Sensitive Modulation of Cortical Neurotransmitters by Transcranial Stimulation. The Journal of Neuroscience. 2009;29: 5202–5206. doi:10.1523/JNEUROSCI.4432-08.2009
79. Antonenko D, Schubert F, Bohm F, Ittermann B, Aydin S, Hayek D, et al. tDCS-Induced Modulation of GABA Levels and Resting-State Functional Connectivity in Older Adults. The Journal of Neuroscience. 2017;37: 4065–4073. doi:10.1523/JNEUROSCI.0079-17.2017
80. Liebetanz D, Nitsche MA, Tergau F, Paulus W. Pharmacological approach to the mechanisms of transcranial DC-stimulation-induced after-effects of human motor cortex excitability. Brain. 2002;125: 2238–2247. doi:10.1093/brain/awf238
81. Nitsche MA, Fricke K, Henschke U, Schlitterlau A, Liebetanz D, Lang N, et al. Pharmacological Modulation of Cortical Excitability Shifts Induced by Transcranial Direct Current Stimulation in Humans. J Physiol. 2003;553: 293–301. doi:10.1113/jphysiol.2003.049916
82. Kuo H-I, Paulus W, Batsikadze G, Jamil A, Kuo M-F, Nitsche MA. Acute and Chronic Noradrenergic Effects on Cortical Excitability in Healthy Humans. International Journal of Neuropsychopharmacology. 2017;20: 634–643. doi:10.1093/ijnp/pyx026
83. Furuya S, Klaus M, Nitsche MA, Paulus W, Altenmüller E. Ceiling Effects Prevent Further Improvement of Transcranial Stimulation in Skilled Musicians. The Journal of Neuroscience. 2014;34: 13834–13839. doi:10.1523/JNEUROSCI.1170-14.2014
84. Bestmann S, de Berker AO, Bonaiuto J. Understanding the behavioural consequences of noninvasive brain stimulation. Trends Cogn Sci. 2015;19: 13–20. doi:10.1016/j.tics.2014.10.003

85. Khan A, Antonakakis M, Vogenauer N, Haueisen J, Wolters CH. Individually optimized multi-channel tDCS for targeting somatosensory cortex. Clinical Neurophysiology. 2022;134: 9–26. doi:10.1016/j.clinph.2021.10.016
86. Lefaucheur J-P, Antal A, Ayache SS, Benninger DH, Brunelin J, Cogiamanian F, et al. Evidence-based guidelines on the therapeutic use of transcranial direct current stimulation (tDCS). Clinical Neurophysiology. 2017;128: 56–92. doi:10.1016/j.clinph.2016.10.087
87. Fregni F, El-Hagrassy MM, Pacheco-Barrios K, Carvalho S, Leite J, Simis M, et al. Evidence-Based Guidelines and Secondary Meta-Analysis for the Use of Transcranial Direct Current Stimulation in Neurological and Psychiatric Disorders. International Journal of Neuropsychopharmacology. 2021;24: 256–313. doi:10.1093/ijnp/pyaa051
88. Soleimani G, Kupliki R, Bodurka J, Paulus MP, Ekhtiari H. How structural and functional MRI can inform dual-site tACS parameters: A case study in a clinical population and its pragmatic implications. Brain Stimul. 2022;15: 337–351. doi:10.1016/j.brs.2022.01.008
89. Buschermöhle Y, Höltershinken MB, Erdbrügger T, Radecke J-O, Sprenger A, Schneider TR, et al. Comparing the performance of beamformer algorithms in estimating orientations of neural sources. iScience. 2024;27: 109150. doi:10.1016/j.isci.2024.109150
90. Schrader S, Antonakakis M, Rampp S, Engwer C, Wolters CH. A novel method for calibrating head models to account for variability in conductivity and its evaluation in a sphere model. Phys Med Biol. 2020;65: 245043. doi:10.1088/1361-6560/abc5aa
91. Antonakakis M, Schrader S, Aydin Ü, Khan A, Gross J, Zervakis M, et al. Inter-Subject Variability of Skull Conductivity and Thickness in Calibrated Realistic Head Models. Neuroimage. 2020;223: 117353. doi:10.1016/j.neuroimage.2020.117353
92. Vieira P, Krause M, Pack C. tACS entrains neural activity while somatosensory input is blocked. 2019. doi:10.1101/691022
93. Misselhorn J, Fiene M, Radecke J-O, Engel AK, Schneider TR. Transcranial Alternating Current Stimulation over Frontal Eye Fields Mimics Attentional Modulation of Visual Processing. The Journal of Neuroscience. 2024;44: e1510232024. doi:10.1523/JNEUROSCI.1510-23.2024
94. Rashbass C. The relationship between saccadic and smooth tracking eye movements. J Physiol. 1961;159: 326–338. doi:10.1113/jphysiol.1961.sp006811
95. Lakens D. Calculating and reporting effect sizes to facilitate cumulative science: a practical primer for t-tests and ANOVAs. Front Psychol. 2013;4. doi:10.3389/fpsyg.2013.00863
96. Benjamini Y, Hochberg Y. Controlling the false discovery rate: a practical and powerful approach to multiple testing. Journal of the Royal Statistical Society. 1995. pp. 289–300. doi:10.2307/2346101
97. Beck AT, Steer RA, Brown GK. Manual for Beck Depression Inventory-II. San Antonio, TX: Psychological Corporation; 1996.
98. Lehrl S. Mehrfachwahl-Wortschatz-Intelligenztest MWT-B [Multiple Choice Vocabulary Test, version B]. 5th ed. Balingen: Spitta; 2005.

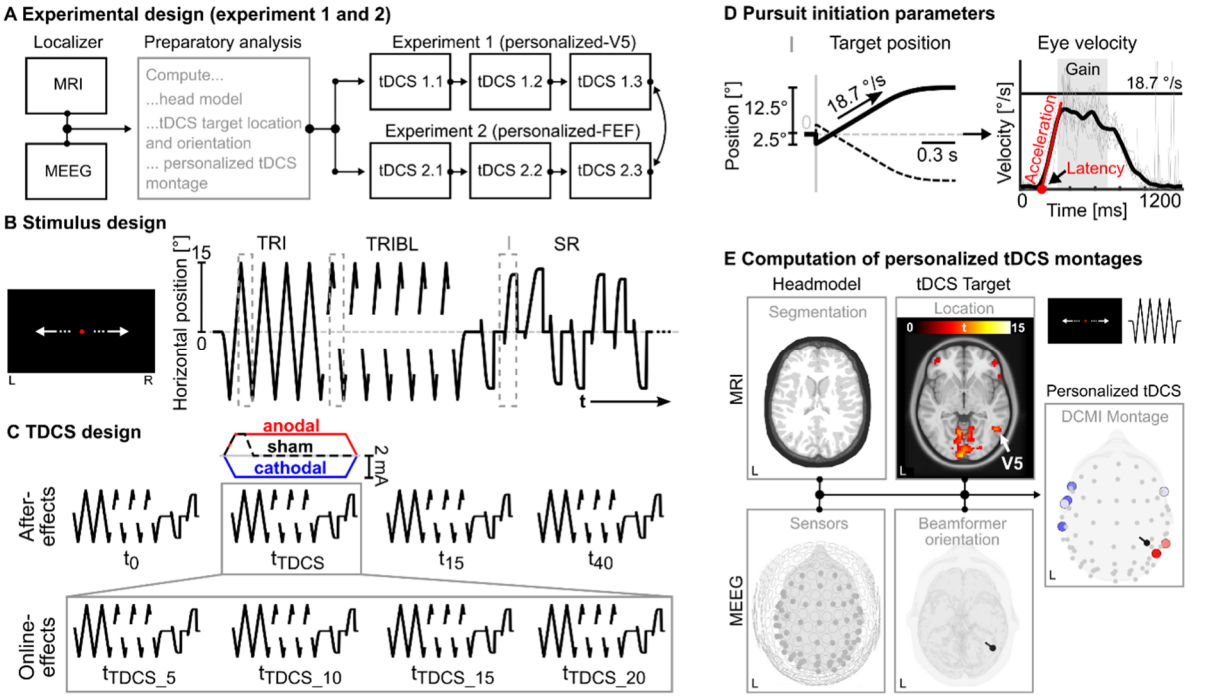

Figure 1. Experimental design. A) Personalized tDCS in experiment 1 and 2 comprised eight experimental sessions on separate days per participant (black boxes). During the first two appointments participants completed MRI and MEEG localizer experiments. Localizer data was used to compute personalized tDCS montages (gray box). Sham, anodal, and cathodal tDCS was applied in three subsequent sessions targeting V5 or FEF. After participants completed the first experiment, three further tDCS sessions were completed for the respective second experiment. The initial assignment to experiment 1 or 2, as well as the order of sham, anodal, and cathodal tDCS within each experiment was counterbalanced across participants. **B)** Horizontally moving visual stimuli were presented. To evaluate the effect of personalized tDCS on different aspects of SP, three tasks were presented, namely continuous SP (TRI), continuous SP with blanking (TRIBL), and foveopetal step-ramp stimuli (I, SR). **C)** In each tDCS session, SP tasks were presented before (t_0), at four timepoints during (t_{TDCS_5}, t_{TDCS_10}, t_{TDCS_15}, t_{TDCS_20}), and 15 (t_{15}) or 40 minutes (t_{40}) after tDCS application. **D)** Pursuit initiation parameters were computed based on the eye tracking data recorded during the step-ramp task. Eye velocities (right) were derived from the eye position (left) as a function of time. Pursuit latency and initial acceleration were computed to define SP initiation performance. Early gain was computed to estimate ongoing SP performance (300 to 700 ms after target motion onset). Target velocity is indicated by a black line at 18.7 °/s. **E)** To compute personalized tDCS montages, structural MRI data were acquired to create a six-compartment segmentation of the individual head (top left). Together with the sensor positions from the combined MEEG session (bottom left), as well as individually calibrated skull conductivity and white matter anisotropy (not shown) individual FEM head models were computed. Individual tDCS targets were defined, using functional MRI data acquired during continuous SP to define the target location in the right hemisphere (top middle, MNI z = -4), and combined MEEG data to define the target orientation (bottom middle). Together the head model and tDCS target information were used to compute personalized tDCS montages with the DCMI algorithm. The workflow to target the area V5 is shown for one exemplary subject.

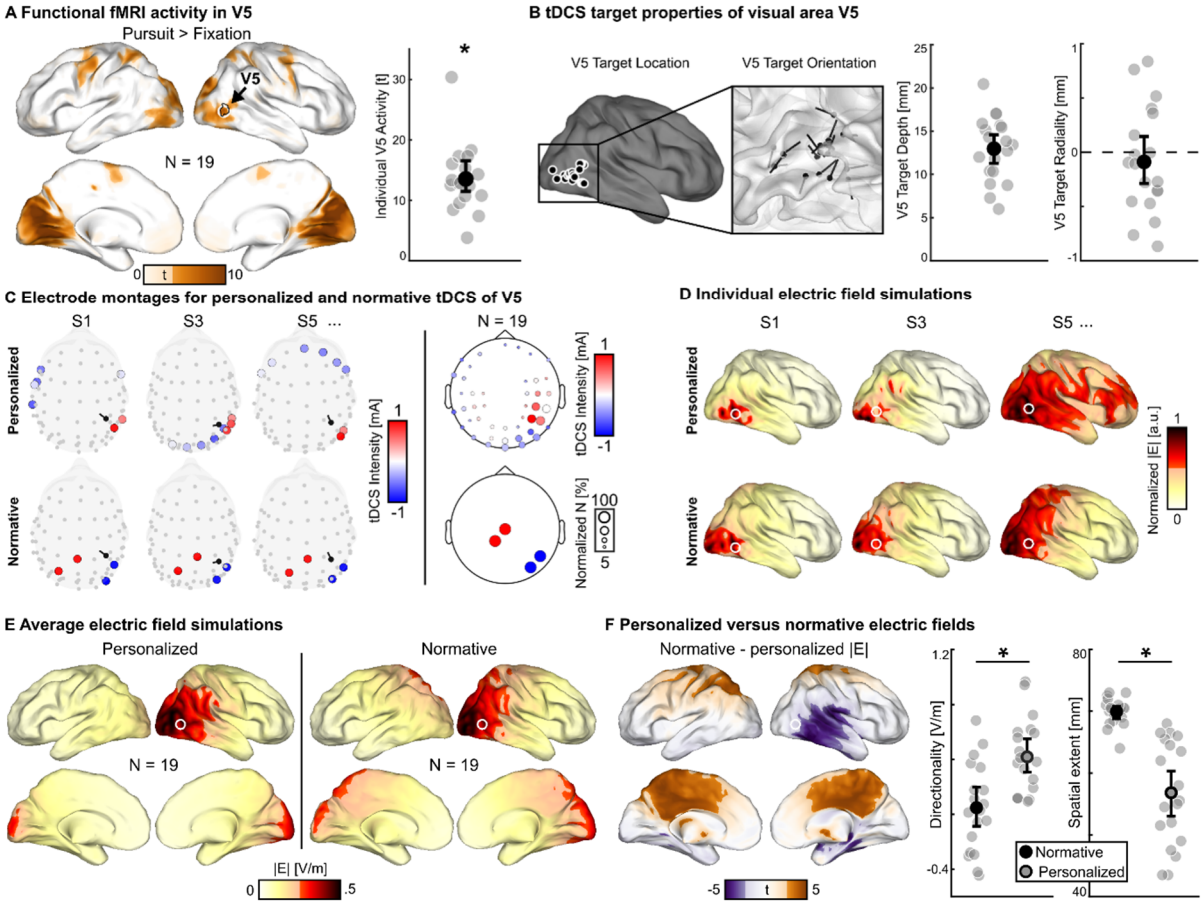

Figure 2. Target V5 and personalized transcranial electric fields. A) Left: Second-level BOLD activity during ongoing SP, compared to fixation, revealed a significant cluster that corresponds to visual area V5. The V5-equivalent cytoarchitectonic area hOc5 (black lines) corresponds to the average coordinate of individual V5 estimates (white circle). FDR-corrected *t*-values are shown, interpolated on the inflated cortical surface of the MNI brain. Right: Individual target V5 activity. Bootstrap mean and confidence interval is depicted together with individual local maxima *t*-values of the first-level statistical contrast of BOLD activity during ongoing SP, compared to fixation. **B)** Target V5 locations (left) are shown on an inflated cortical surface of the MNI brain. Estimated V5 orientations (middle) are shown together with the white matter surface of the MNI brain. Right: V5 target depth relative to the inner skull surface and radiality (1/-1 = radial/anti-radial, 0 = tangential) bootstrap means and confidence intervals are depicted together with individual values. **C)** Personalized tDCS montages targeting individual V5 (top) and normative tDCS montages over V5 (bottom) are shown for three exemplary subjects (left; top view). Topographical representations for the whole sample are shown for personalized (top right) and normative tDCS montages (bottom right). Circle sizes illustrate the normalized number of individual montages that comprised the respective electrode, color illustrates the average tDCS intensity per electrode across the whole sample. **D)** Electric field simulations for the same three subjects and personalized (top) and normative (bottom) tDCS montages, respectively. Normalized electric field intensities |**E**| were interpolated on the inflated right cortical surface of the MNI brain, with values below 50% of the maximal intensity masked (light colors). Individual tDCS target locations in the right V5 are indicated by white circles. **E)** Lateral and medial view of average simulated electric fields for personalized (left) and normative (right) tDCS interpolated on the inflated cortical surface of the MNI brain, with values below 50% of the maximal intensity masked (light colors). The average tDCS target location in the right V5 is indicated by a white circle, respectively. **F)** Left: Comparison between personalized and normative simulated electric fields revealed increased electric field intensities in bilateral parietal and medial brain regions for normative tDCS, whereas personalized electric field intensities were increased in right temporal, and parietal regions anterior to the average V5 location (white circle), corresponding to more anterior individual V5 locations (compare panel B). Lateral and medial view of significant *t*-values are shown (bold colors), with *t*-values corresponding to FDR-corrected *p*-values > 0.05 masked (light colors). Right: Directionalities in the target V5 for electric fields induced by normative tDCS were significantly smaller and spatial extent of the electric field across the cortex was significantly larger, compared to personalized target directionalities and spatial extent. Bootstrap means and confidence intervals are depicted together with individual values. * indicate $p < .05$.

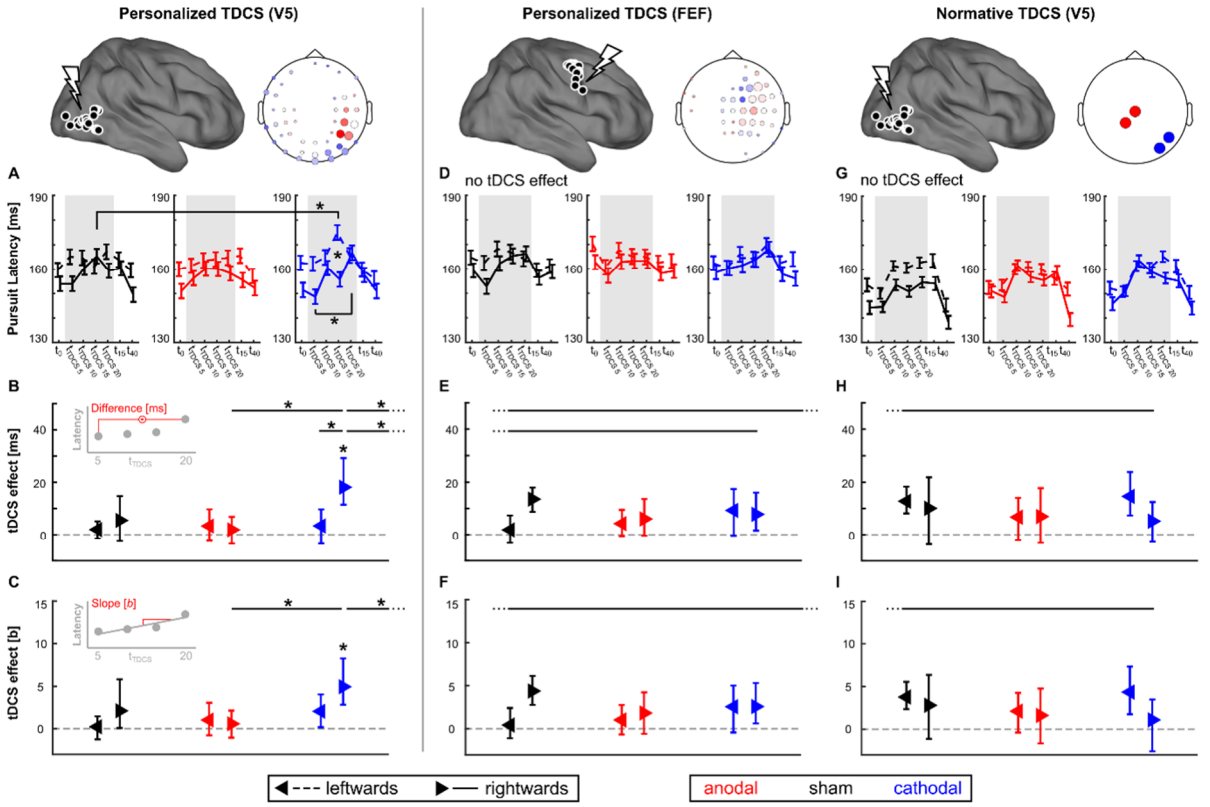

Figure 3. tDCS effects on SP latencies during the step-ramp task. A) to C) In experiment 1 (V5-personalized), significant modulation of SP latencies during the SR task by personalized cathodal tDCS targeting V5 was observed. An effect was observed across **A)** all timepoints (t_0, t_{TDCS_5}, t_{TDCS_10}, t_{TDCS_15}, t_{TDCS_20}, t_{15}, t_{40}). Gray shaded boxes indicate the 20 minutes tDCS interval. LMM analyses revealed an online effect of personalized cathodal tDCS with significantly delayed latencies for ipsiversive (i.e., rightwards) SP during the last timepoint (t_{TDCS_20}), compared to the first (t_{TDCS_5}) timepoint during t_{TDCS}. **B)** tDCS effect estimated as difference between t_{TDCS_20} versus t_{TDCS_5} is plotted for sham, anodal, and cathodal tDCS conditions, as well as leftwards and rightwards SP latencies, respectively (bootstrap mean ± confidence interval). Top left inset illustrates the computation of the difference tDCS effect. Follow-up analysis of difference tDCS effects reveals significant differences for personalized cathodal tDCS for rightward SP latencies, compared to leftward SP latencies of the same tDCS condition, rightward SP latencies during anodal tDCS, as well as an increased difference tDCS effect of personalized cathodal tDCS targeting V5, compared to personalized tDCS targeting FEF and normative cathodal tDCS over V5. **C)** tDCS effect estimated as slope of robust regression across all t_{TDCS} timepoints is plotted for sham, anodal, and cathodal tDCS conditions, as well as leftwards and rightwards SP latencies, respectively (bootstrap mean ± confidence interval). Top left inset illustrates the computation of the slope tDCS effect. Slope estimates of tDCS effects are significantly increased for personalized cathodal tDCS targeting V5, compared to anodal tDCS, as well as normative cathodal tDCS over V5. **D) to F)** No specific tDCS effects were observed for personalized tDCS targeting the right FEF. **G) to I)** No specific tDCS effects were observed for normative tDCS over the right V5. * indicate $p < .05$ (Bonferroni-corrected). tDCS targets and topographical illustration of the cathodal tDCS montage are depicted for the experiment 1 (V5-personalized, top left), experiment 2 (FEF-personalized, top middle), and experiment 3 (V5-normative, top right), respectively.

Table 1. Sample information for the personalized and the normative tDCS participants. For both samples sample size (N), age (M ± SD), gender (frequencies), handedness (frequencies), raw values for the Beck Depression Inventory (BDI-II 126) and percentile ranks for the Multiple Choice Vocabulary Test (MWT-B 127) are provided. F = female, M = male, R = right-handed, L = left-handed, A = ambidextrous.

Parameter	Personalized tDCS targeting V5 and FEF	Normative tDCS over V5
Sample size	19	19
Age	26.2 ± 7.6	25.5 ± 7.1
Gender	F: 11, M: 8	F: 11, M: 8
Handedness	R: 16, L: 2, A: 1	R: 16, L: 3
BDI-II	1.7 ± 2.2	1.4 ± 1.2
MWT-B	47.7 ± 19.6	55.2 ± 20
Days between tDCS sessions	7.9 ± 7.8	8.5 ± 4.7

Table 2. Descriptive smooth pursuit performance. Great grand average pursuit performance for experiment 1 (V5-personalized), experiment 2 (FEF-personalized), and experiment 3 (V5-normative). Mean (± SD) is reported for the respective parameters of continuous pursuit (TRI), continuous pursuit with blanking (TRIBL), and foveopetal step-ramps (SR). a.u. = arbitrary unit.

Task	Parameter	Unit	Experiment 1 (V5-personalized)	Experiment 2 (FEF-personalized)	Experiment 3 (V5-normative)
TRI	Maintenance gain	a.u.	0.957 ± 0.042	0.936 ± 0.044	0.941 ± 0.039
TRIBL	Preblank gain	a.u.	0.839 ± 0.108	0.819 ± 0.108	0.814 ± 0.112
	Deceleration latency	ms	130 ± 17	134 ± 22	134 ± 19
	Deceleration	$°/s^2$	47 ± 9	46 ± 9	54 ± 7
	Resdidual gain	a.u.	0.439 ± 0.223	0.425 ± 0.216	0.314 ± 0.145
	Re-acceleration latency	ms	-132 ± 35	-136 ± 39	-136 ± 39
	Re-acceleration	$°/s^2$	27 ± 10	26 ± 10	26 ± 9
	Postblank gain	a.u.	0.811 ± 0.125	0.786 ± 0.106	0.731 ± 0.145
SR	Pursuit latency	ms	160 ± 13	163 ± 13	154 ± 11
	Acceleration	$°/s^2$	128 ± 34	126 ± 33	109 ± 29
	Early maintenance gain	a.u.	0.827 ± 0.086	0.809 ± 0.087	0.799 ± 0.094

Table 3. Personalized tDCS targeting V5 induces online effects modulating SP initiation. Results of LMM analysis indicate significant transient modulation of SP initiation, specifically pursuit latency and initial acceleration during SR, by personalized tDCS targeting V5 during the tDCS application (online effects, i.e. considering timepoints t_{TDCS_5}, t_{TDCS_10}, t_{TDCS_15}, and t_{TDCS_20}). TRI = continuous pursuit, TRIBL = continuous pursuit with blanking, SR = step-ramp. * indicate *p*-values < .05.

Task	Parameter	tDCS condition		tDCS condition * Timepoint		tDCS condition * Direction		tDCS condition * Timepoint * Direction	
		F	*p*	F	*p*	F	*p*	F	*p*
TRI	Maintenance gain	1.35	.263	0.26	*.955*	1.71	*.183*	0.63	*.705*
TRIBL	Preblank gain	**6.09 ***	***.003***	1.31	*.252*	0.55	*.58*	0.28	*.948*
	Deceleration latency	1.59	.207	0.19	*.98*	1.37	*.257*	0.28	*.945*
	Deceleration	2.61	.077	0.15	*.989*	0.12	*.886*	0.86	*.521*
	Residual gain	0.32	.73	0.26	*.955*	0.54	*.586*	0.11	*.995*
	Re-acceleration latency	**4.79 ***	***.01***	0.7	*.648*	0.77	*.467*	1.1	*.36*
	Re-acceleration	0.02	.978	0.28	*.945*	0.39	*.675*	0.59	*.736*
	Postblank gain	**3.24 ***	***.041***	0.39	*.887*	0.02	*.982*	0.46	*.836*
SR	Pursuit latency	0.63	.534	1.11	*.355*	0.79	*.456*	**2.7 ***	***.015***
	Initial acceleration	0.29	.751	0.77	*.596*	0.25	*.78*	**2.56 ***	***.02***
	Early maintenance gain	**4.74 ***	***.01***	0.41	*.87*	0.15	*.862*	0.74	*.62*

Table 4. No tDCS after-effects. Results of LMM analysis do not indicate a significant modulation of SP parameters after personalized tDCS targeting V5 (after effects, i.e. considering timepoints t_0, t_{15}, and t_{40}). TRI = continuous pursuit, TRIBL = continuous pursuit with blanking, SR = step-ramp. * indicate *p*-values < .05.

Task	Parameter	tDCS condition		tDCS condition * Timepoint		tDCS condition * Direction		tDCS condition * Timepoint * Direction	
		F	*p*	F	*p*	F	p	F	*p*
TRI	Maintenance gain	0.71	*.491*	1.56	*.159*	0.05	*.954*	0.19	*.979*
TRIBL	Preblank gain	0.45	*.638*	1.19	*.312*	1	*.369*	0.46	*.838*
	Deceleration latency	0.87	*.42*	0.58	*.748*	0.06	*.943*	0.9	*.492*
	Deceleration	0.18	*.836*	0.37	*.896*	0.92	*.4*	0.31	*.934*
	Residual gain	0.51	*.599*	0.27	*.95*	0.1	*.902*	0.15	*.99*
	Re-acceleration latency	**6.7 ***	***.002***	1.94	*.074*	0.08	*.924*	0.54	*.782*
	Re-acceleration	0.44	*.644*	0.11	*.995*	0.62	*.542*	1.42	*.207*
	Postblank gain	1.34	*.264*	1.14	*.342*	0.04	*.963*	0.15	*.989*
SR	Pursuit latency	0.72	*.487*	0.53	*.786*	0.07	*.936*	0.92	*.484*
	Initial acceleration	0.28	*.755*	0.48	*.824*	0.01	*.989*	0.43	*.857*
	Early maintenance gain	1.36	*.259*	0.83	*.545*	0.24	*.784*	0.14	*.991*

1074